2009

Novel optofluidic sensor systems for quantitative chemical imaging and on-chip sensor calibration

Jongwon Park

Recommended Citation

Park, Jongwon, "Novel optofluidic sensor systems for quantitative chemical imaging and on-chip sensor calibration" (2009). *Doctoral Dissertations*. 2225.
https://scholarsmine.mst.edu/doctoral_dissertations/2225

NOVEL OPTOFLUIDIC SENSOR SYSTEMS FOR

QUANTITATIVE CHEMICAL IMAGING AND

ON-CHIP SENSOR CALIBRATION

by

JONGWON PARK

A DISSERTATION

Presented to the Faculty of the Graduate School of the

MISSOURI UNIVERSITY OF SCIENCE & TECHNOLOGY

In Partial Fulfillment of the Requirements for the Degree

DOCTOR OF PHILOSOPHY

in

ELECTRICAL ENGINEERING

2009

Approved by

Chang-Soo Kim, Advisor

Cheng Hsiao Wu

Minsu Choi

Matthew O'Keefe

David Henthorn

PUBLICATION DISSERTATION OPTION

This dissertation consists of the following three articles that have been submitted for publication, or will be submitted for publication as follows:

Pages 12 - 31 were submitted for publication in IEEE SENSORS JOURNAL.

Pages 32 - 47 are intended for submission to SENSORS AND ACTUATORS B: CHEMICAL.

Pages 48 - 62 are intended for submission to SENSORS AND ACTUATORS B: CHEMICAL.

ABSTRACT

The design, fabrication and characterization of optofluidic biosensor systems for quantitative oxygen imaging with a color charge-coupled device (CCD) camera as well as on-chip self-calibration of sensors utilizing gas bubbles was investigated. This dissertation was prepared in publication format. The first and second papers demonstrate that color imaging devices can be used in quantitative chemical analysis. The final paper explores the feasibility of using electrolytically generated bubbles for a novel functionality of reagentless, on-chip, *in situ* calibration of optical biosensors. Work in the first paper includes the use of a color CCD camera for fluorescence intensity imaging. This involves extracting the red color element to determine the dissolved oxygen content from the color image of a sample. The linearity and sensitivity of oxygen detection based on the red intensity analysis was improved to those of spectrometric measurement and total color intensity analysis. In the second paper, the color extraction technique used in the dissolved oxygen sensor was extended to gaseous oxygen detection to eliminate the need of optical filters and replace the blue light emitting diode (LED) excitation source with a general broad-band white LED. This new method has potential applications in multi-analyte monitoring and simultaneous structural/functional imaging of biological samples with a single broad-band light source. In the final paper, a double-layered optofluidic system was developed to demonstrate on-chip, self-calibration of dissolved oxygen sensor. A multilayers of dry film resist was used for preparing a 3-D fluidic structure. A thin black polydimethylsiloxane membrane was used for oxygen diffusion and optical isolation. The sensor calibration result with the on-chip bubble was shown to be in good agreement with that of standard calibrants.

ACKNOWLEDGMENTS

The work in this dissertation would never have been possible without the support and guidance of my advisor, Dr. Chang-Soo Kim. His direction in all aspects of my graduate work was invaluable and will be forever appreciated.

I wish to express my sincere thanks to Prof. Dr. Cheng-Hsiao Wu, Prof. Dr. David B. Henthorn, Prof. Dr. Minsu Choi, and Prof. Dr. Matthew O'Keefe for their valuable discussions and help throughout this study.

I also wish to express my endless thanks to my family especially to my spouse Juryun Kim, daughter Flora, and son Jason for their patience, moral support and encouragement.

Appreciation is extended to my friends in the Missouri University of Science and Technology.

TABLE OF CONTENTS

LIST OF ILLUSTRATIONS

LIST OF TABLES

SECTION

1. INTRODUCTION

Molecular oxygen is one of major species for the metabolism of organisms and also for a majority of biochemical processes. Consequently, there are many application fields where the oxygen determination is critical. This dissertation focuses on the design, fabrication and characterization of optofluidic biosensor systems for oxygen quantification with a color charge-coupled device (CCD) camera and an on-chip self-calibrator utilizing electrochemically generated gas bubbles.

1.1 OPTICAL OXYGEN SENSORS

Optical oxygen sensors are gradually replacing their electrochemical counterparts because they do not consume oxygen during measurement and do not interfere with other electrical devices. Additionally, optical oxygen sensors are particularly useful in the area of biological oxygen monitoring because of their potential for noninvasive and remote detection and system miniaturization.

The luminescence quenching by oxygen was first introduced during 1930's by Kautsky and Hirsch [1, 2] as explained in Figure 1.1. The collision between the indicator molecule (i.e., excited luminophore) and the quencher (i.e., oxygen) causes the luminophore to be in a radiationless deactivated state. After the collision, energy transfer takes place from the luminophore to oxygen which consequently is transferred from its ground state (triplet state) to its excited singlet state. Eventually, the luminophore does not emit luminescence and a change in the intensity of luminescence is measured. For the oxygen measurement, the luminophore is usually immobilized in an oxygen permeable membrane. Bergman demonstrated the first complete optical oxygen sensor system in 1968 based on this detection mechanism [3]. The system consisted of a UV light source, an oxygen sensitive fluorescent layer embedded in a porous glass film, and a photodectector. After this pioneering development, the majority of optical oxygen sensors employ a structure wherein oxygen-sensitive luminophores were immobilized at the tip

of the optical fibers (usually called optode or optrode) and fluorescence intensity or decay time was measured [4].
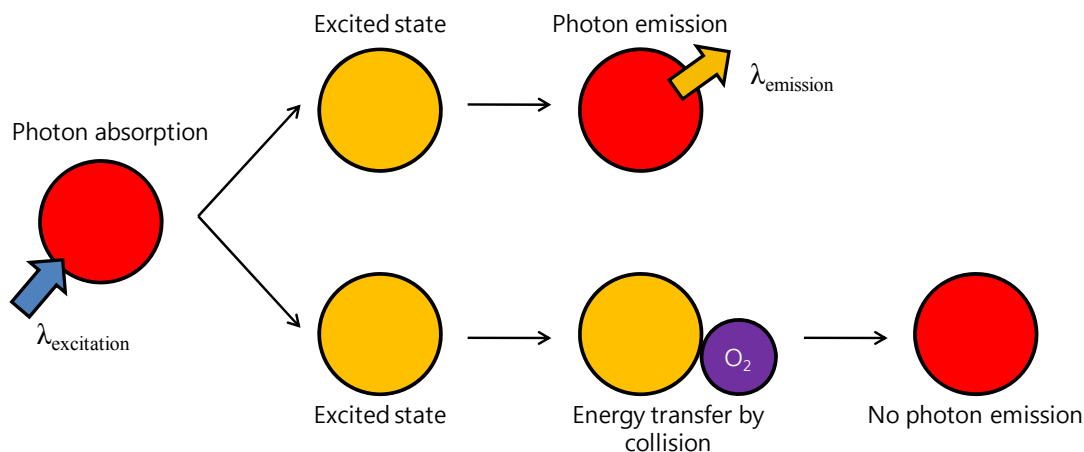
Figure 1.1. The principle of dynamic luminescence quenching by oxygen.

Many kinds of oxygen-sensitive luminophores are available including polycyclic aromatic hydrocarbons, transition metal complexes of Ru(II), Os(II) or Rh(II), and phosphorescent porphyrins containing Pt (II) or Pd(II). Ru(II) complexes have been the most widely used for fluorescence oxygen sensors because of their good photostability, high quantum yield, large Stokes shift, and wide dynamic range of ratio of fluorescence intensities in the absence and presence of oxygen [5, 6]. For the oxygen permeable membrane, polymer films such as silicone, organic glassy polymers including polystyrene and poly(methylmethacrylate), fluoropolymers, and cellulose derivatives have been used [6]. Among them, (poly)ethylene glycol (PEG) is a very promising material for the use as a biological sensor membrane due to its hydrophilic property and high permeability towards oxygen. It is also biocompatible and optically transparent in nature. The fluorescence quenching of Ru(II)-complexes embedded in photopatterned PEG hydrogels or commercial sol-gel layers was utilized as the basic oxygen detection mechanism for this dissertation.

1.2 PHOTOPATTERNING OF OPTICAL SENSOR ARRAY

In many applications of bio-micro-electro-mechanical system (bioMEMS) devices, there is a large need of microscopically patterned optical sensor membranes that can measure chemical parameters in a small local area. Patternable optical membranes also allow us to fabricate optode arrays for two-dimensional chemical mapping or multi-analyte sensing. Most of the oxygen-sensitive sensors are, however, non-patternable by photolithography and very little progress has been made towards producing patternable optical sensors. For this work to be feasible, a membrane matrix material is needed that is transparent, oxygen-permeable and photopatternable.

In this dissertation, an effort has been made to produce small patterns of thin oxygen sensitive membranes using photopatternable PEG hydrogel. Patterning a thin PEG layer is possible through the addition of a photoinitiator to the PEG-based precursor. The resulting hydrogel physically entraps the oxygen-sensitive Ru(II)-complexes. Revzin et al. photopatterned 7 to 600 μm diameter cylindrical structures by adding 2,2-dimethoxy-2-phenylacetophenone photoinitiator to PEG [7]. By controlling the molecular weight of the macromer PEG, they varied the height of the structures from 2 to 12 μm. O'Neal et al. also combined a photopatternable PEG matrix with ruthenium complexes to fabricate optical oxygen sensor array [8]. A similar procedure was used in this dissertation to demonstrate original research ideas.

1.3 APPLICATION OF COLOR CCD TO QUANTITATIVE CHEMICAL IMAGING

The spectrometer is the most commonly used instrument for luminescence-based measurements although it is expensive and needs a trained person to use it. Also it is limited to one-dimensional sample analysis by its nature. Two-dimensional oxygen measurement, however, requires multiple point detection simultaneously to eliminate the inconvenience of successive reading of individual sensors.

To solve the above problems, photometric methods have been introduced to conduct the quantitative two-dimensional chemical mapping from the image of optical

oxygen sensor arrays taken by solid-state imaging devices [9, 10]. Mostly, monochrome CCD cameras, with optical filters if necessary, were used for luminescence imaging in which the overall intensities of all colors were taken into consideration to estimate the oxygen content. Until recently, however, color CCDs have rarely been used for imaging oxygen sensor arrays, although it is useful to analyze the spectral contents of an image. Part of the problem with using color CCDs is that they are inherently biased towards the detection of green light in order to mimic the human eye [11]. Most color CCDs accomplish this by utilizing Bayer masks over the CCD surface to split red, blue, and green colors spatially [12]. Figure 1.2 shows the Bayer color filter arrangement on the color CCD [13]. Each pixel element is composed of four sub-pixels. One sub-pixel receives red, one receives blue, and the other two sub-pixels detect green intensity to obtain all the color information for the whole pixel. This means that the CCD camera is more sensitive to green because it has more pixel elements for green color detection.

With this background information in mind, a red color analysis method is proposed herein to eliminate unnecessary and distorted information from the color CCD image of a sensor array for improving the oxygen sensitivity in quantitative imaging.
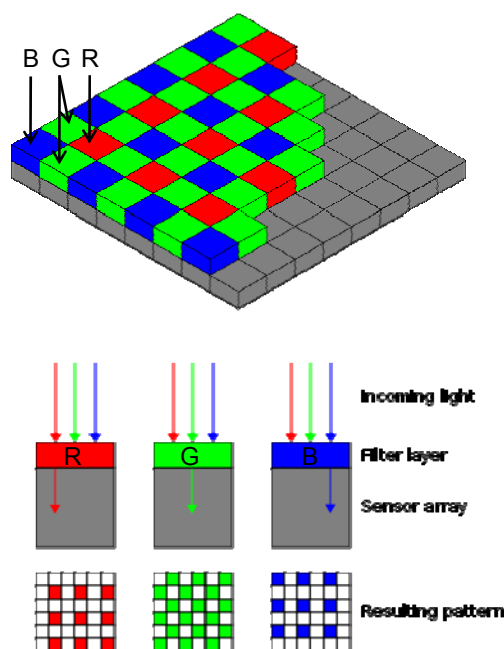
Figure 1.2. The Bayer arrangement of color filters on the pixel array of a color CCD (after [13]).

1.4 SELF-CALIBRATION USING ELECTROLYTIC GAS BUBBLES

Nearly all biochemical sensors exhibit instabilities such as baseline drift and sensitivity degradation. Figure 1.3 shows the concept of *in vitro*, *in vivo*, and *in situ* calibration/diagnosis techniques for the biochemical sensors that is inevitable for continuous monitoring operation. Most of the current biochemical sensor developments, however, have been mainly focused on the miniaturization of devices and the exploratory use of new functional materials. The importance and needs of innovative methods for *in situ/in vivo* calibration [14] and self-calibration [15] have been pointed out, but only little technological breakthrough has been made till now. One report introduced an interesting concept of "OR-OR" switch for the self-calibration of fluorescence sensor which requires two-band wavelength-ratiometric measurement using rapid reversible single dye molecule [16]. However, a sampling for "gold standard" analysis by laboratory equipment for *in vivo* measurement (shown in Figure 1.3 (b)) and external calibration medium injections for the *in situ* measurement (shown in Figure 1.3 (c)) are still the most common ways for sensor calibration provided such a single dye molecule is not available in every case. It should be noted that all general concepts of *in vivo* and *in situ* calibration methods require a considerable amount of laborious human attendance and involve externally coupled bulky mechanical and fluidic components.

For this purpose, this dissertation introduces a unique method utilizing on-chip gas bubbles (i.e., a pair of oxygen and hydrogen) which are generated electrochemically [17, 18]. The electrolysis reactions occurring at the anodic and cathodic bubble generation electrodes are as follows:

$$2H_2O \rightarrow 4H^+ + 4e^- + O_2 \text{ (at anodic electrode)} \tag{1}$$
$$4H_2O + 4e^- \rightarrow 4OH^- + 2H_2 \text{ (at cathodic electrode)} \tag{2}$$
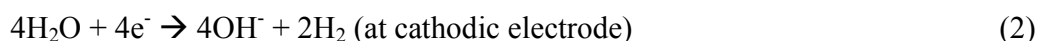
In a previous research as shown in Figure 1.4, the optical oxygen sensor was provided with local environment depending on the location of the bubbles and the solution. The high-point diagnosis/calibration microenvironment was established with an oxygen bubble (100% oxygen) and the low-point environment with a hydrogen bubble (0%
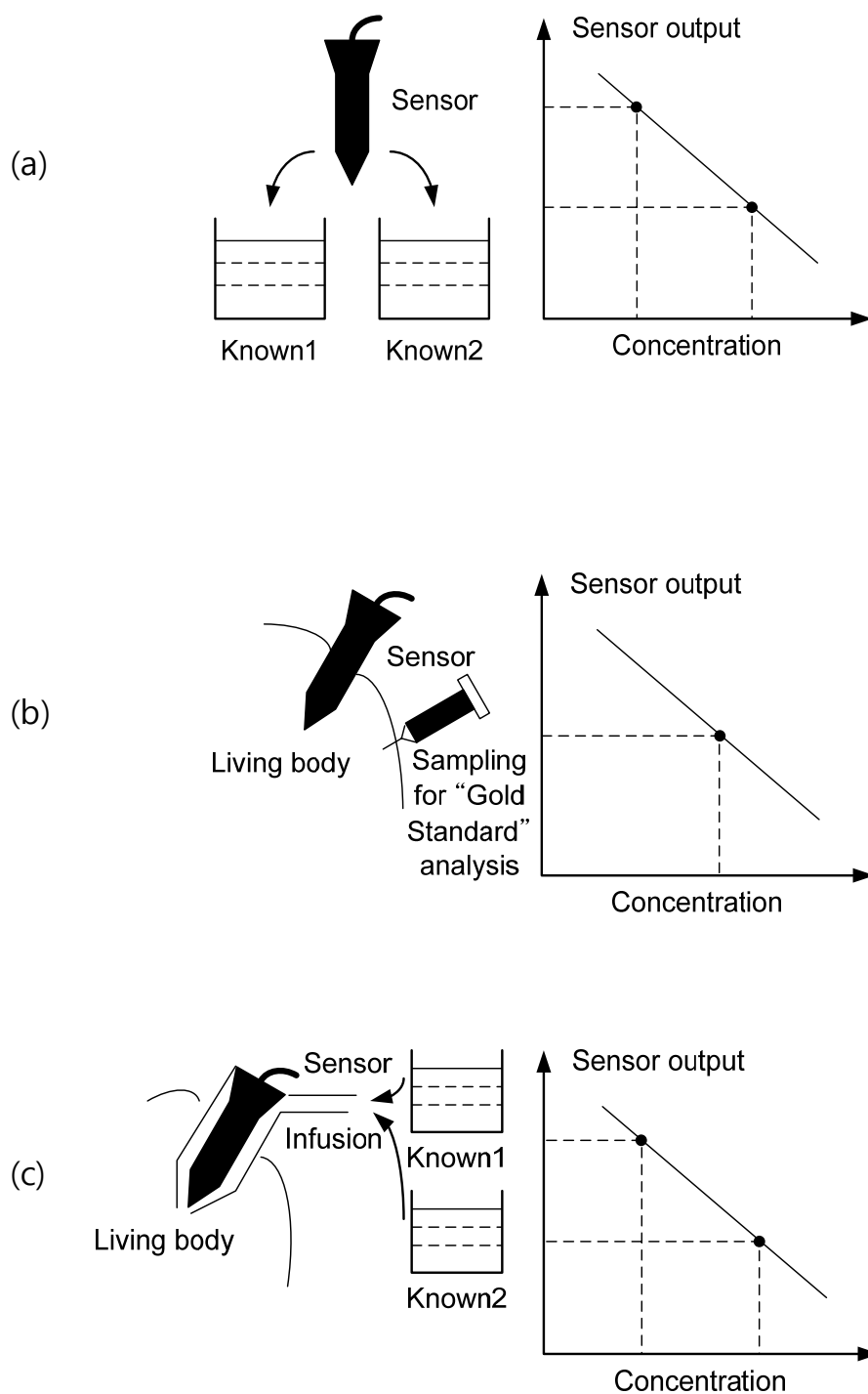
Figure 1.3. Sensor calibration and diagnosis techniques. (a) *in vitro* calibration in the known calibrants before measurements, (b) *in vivo* calibration by adjusting the sensor output with results from "Gold Standard" analysis of withdrawn sample, and (c) *in situ* calibration by infusing the calibrants with a flow system
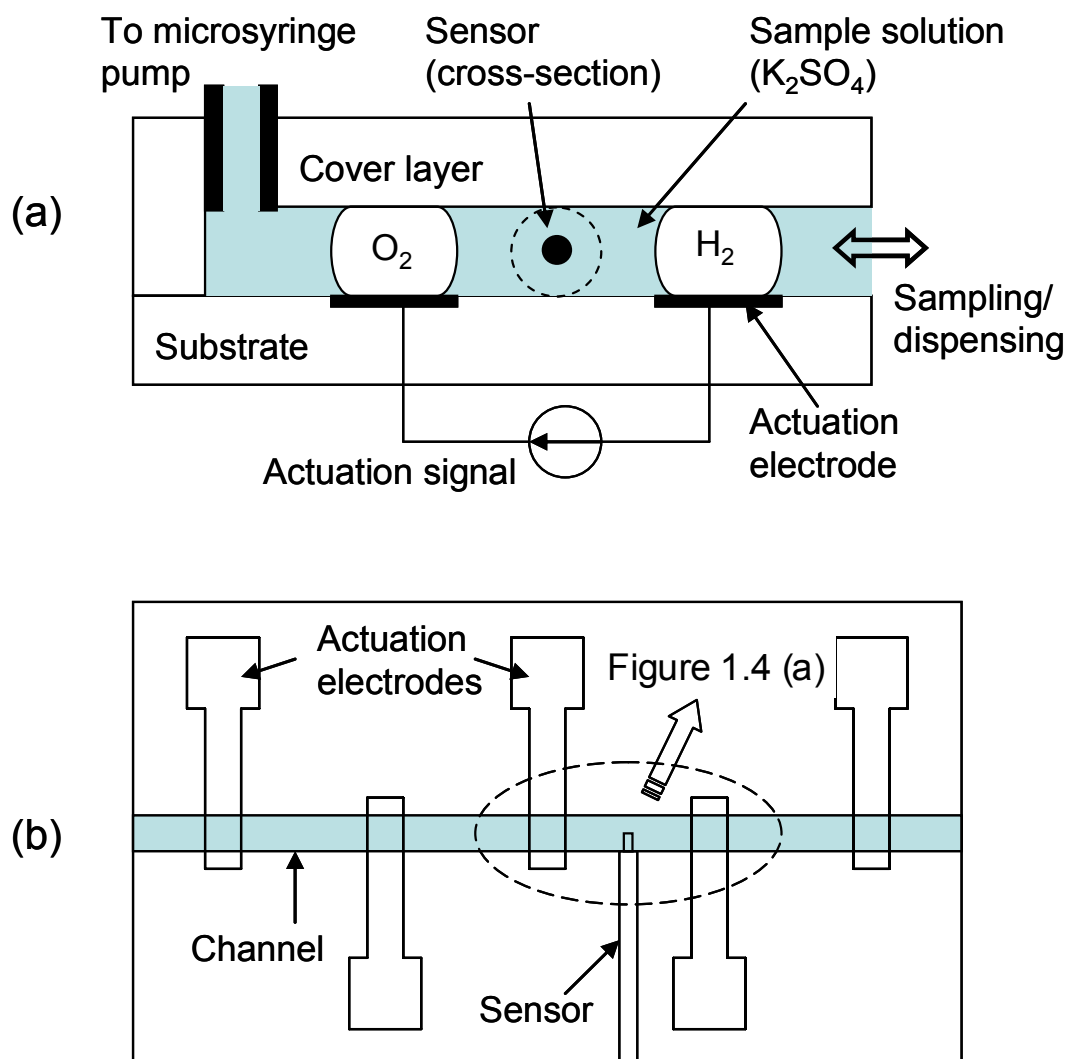
Figure 1.4. The fluidics chip for an on-chip 2-point *in situ* self-calibration of oxygen microsensor by water electrolysis. A pair of electrochemically generated bubbles provides microenvironments for the high-point procedure with the oxygen bubble (100% oxygen) and the low-point procedure with the hydrogen bubble (0% oxygen). (a) simplified cross-section, and (b) layout of the system [17].

oxygen), respectively. In the case of glucose or lactate sensor (shown in Figure 1.5), a one-point sensor calibration (i.e., zero value) was performed by manipulating the hydrogen-gas bubble. The proposed glucose and lactate sensors were based on the amperometric detection of hydrogen peroxide generated by the glucose (or lactate) oxidase-catalyzed oxidation of β-D-glucose (or L-lactate). These enzymes catalyze the following reactions:

$$\beta - D - \text{Glucose} + O_2 \xrightarrow{\quad GOD \quad} \text{Gluconic acid} + H_2O_2 \quad (\text{GOD: Glucose oxidase}) \quad (3)$$

$$\text{L-Lactate} + O_2 \xrightarrow{\quad LOD \quad} \text{Pyruvate} + H_2O_2 \quad (\text{LOD: Lactate oxidase}) \qquad (4)$$
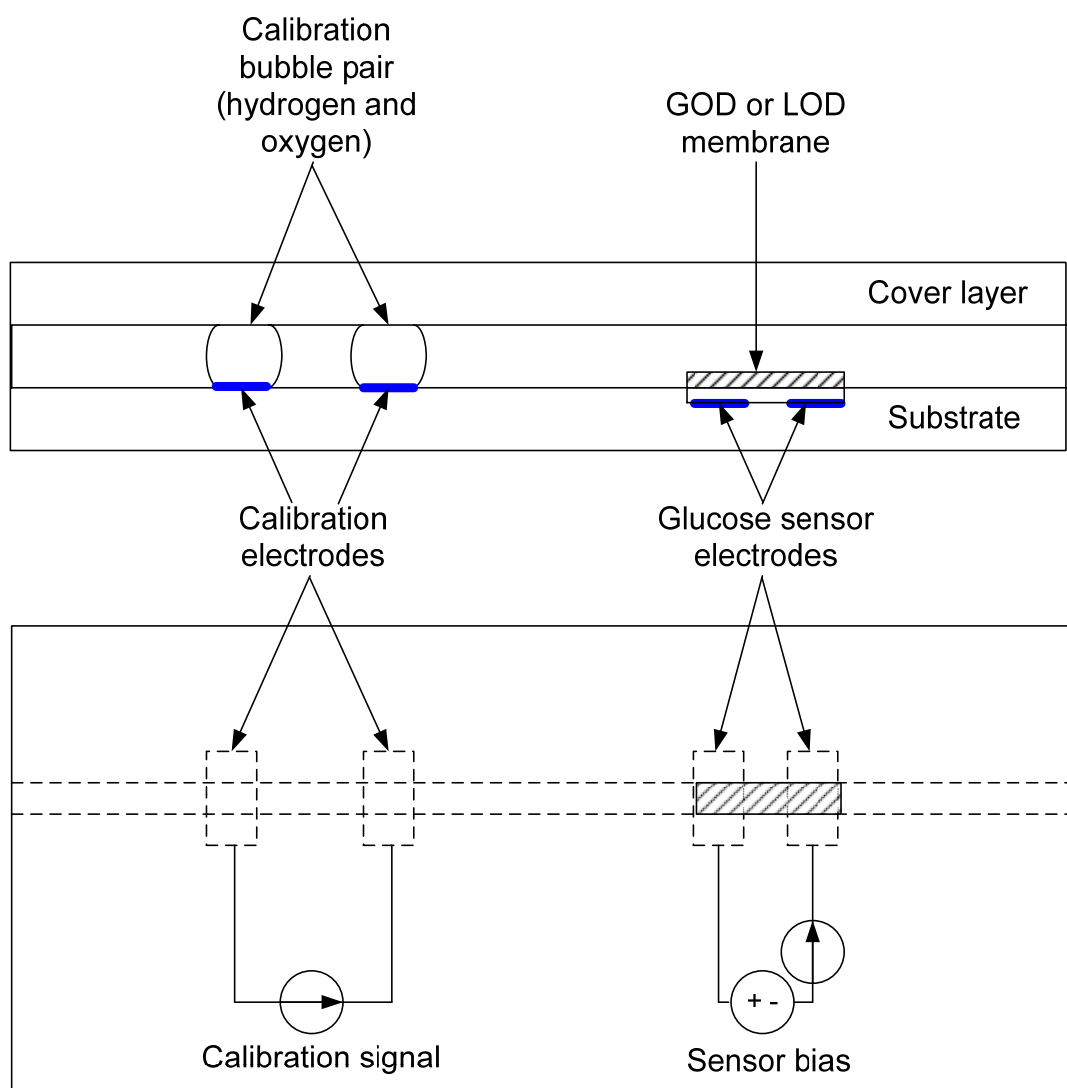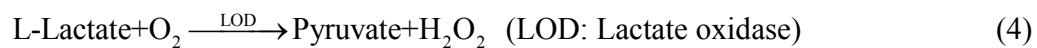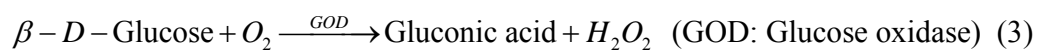
Figure 1.5. The fluidic chip for built-in one-point *in situ* calibration of glucose or lactate sensor using water electrolysis. Electrochemically generated bubbles provide microenvironment for the one-point calibration and sensitivity-enhancement procedure. (a) simplified cross section and (b) layout of the system [18].

When the sensor was surrounded by the hydrogen bubble, this oxygen-free environment prevented the enzyme reaction because the enzyme reaction needs oxygen. This technique resulted in a virtual glucose (or lactate)-free microenvironment for low-point calibration. On the contrary, the oxygen bubble was used for the sensitivity enhancement. This artificial constant oxygen microenvironment provided enough oxygen for enzyme reaction such that the enzyme reaction is not limited by the oxygen tension in the sample solution. In above previous method, the generated hydrogen or oxygen bubble was shifted and made contact with the biosensor placed in a microfluidic channel in such a way that the biosensor tip was completely surrounded by the respective bubble. Tests based on this procedure sometimes showed inconsistent and erroneous results. It was considered that the bubbles were drying up the enzyme layer located at the biosensor tip during the calibration phase. Another possible reason is that the reaction byproducts accumulated within the enzyme layer since it is isolated from the bulk solution by the surrounding bubble. An improved assembly design was introduced for optical dissolved oxygen sensor self-calibration in this dissertation. The bubble generating chamber and the sensing chamber were separated by a black gas permeable polydimethylsiloxane (PDMS) membrane for oxygen diffusion and optical isolation. A PDMS was chosen as diffusion membrane due to its high oxygen permeability [19]. Moreover, the dissolved oxygen sensor (commercial oxygen-sensitive patch) is integrated to the sensor chip instead using externally coupled optical oxygen sensor to implement fully integrated microfluidic system.

1.5 ORGANIZATION

The three papers attached in this dissertation consist of the concepts and backgrounds described in these sections (i.e., $1.1 - 1.4$). Table 1.1 lists the contents of each paper. The performance of color CCD as a quantitative chemical detector was discussed and compared with that of traditional spectrometry in paper 1 and 2 while the feasibility study of on-chip self-calibration is the main focus of paper 3. Both the photopatterned hydrogel and commercial oxygen-sensitive patches (RedEye^{TM} , RE-FOX-8, 8 mm diameter, Ocean Optics) were used to demonstrate the research ideas.

Table 1.1. Contents of papers.

Sections in the Introduction chapter	Paper
- Optical oxygen sensors	1, 2, 3
- Photopatterning of optical sensor array	1
- Application of color CCD in quantitative chemical detection	1, 2
- Self-calibration using electrolytic gas bubbles	3

1.6 REFERENCES

[1]   H. Kautsky and A. Hirsch, "Interactions of Excited Dye Molecules and Oxygen," Berichte der Deutschen Chemischen Gesellschaft, 64, 2677, 1931.

[2]   H. Kautsky, "Quenching of Luminescence by Oxygen," Transactions of the Faraday Society, 35, 216-219, 1939.

[3]   I. Bergman, "Rapid-response Atmospheric Oxygen Monitor based on Fluorescence Quenching," Nature, 218, 396, 1968.

[4]   H. H. Hesse, East Germany Patent, 106086, 1974.

[5]   Y. Amao, "Probes and Polymers for Optical Sensing of Oxygen," Microchimica Acta, 143, 1-12, 2003.

[6]   A. Mills, "Optical Oxygen Sensors," Platinum Metals Review, 41, 115-127, 1997.

[7]   A. Revzin, R. J. Russell, V. K. Yadavalli, W. Koh, C. Deister, D. D. Hile, M. B. Mellott, and M. V. Phishko, "Fabrication of Poly(ethylene glycol) Hydrogel Microstructures Using Photolithography," Langmuir, 17, 5440-5447, 2001.

[8]   D. P. O'Neal, M. A. Meledeo, J. R. Davis, B. L. Ibey, V. A. Gant, M. V. Pishko and G. L. Coté, "Oxygen Sensor Based on the Fluorescence Quenching of a Ruthenium Complex Immobilized in a Biocompatible Poly(ethylene glycol) Hydrogel," IEEE Sensors Journal, 4, 728–734, 2004.

[9]   R. N. Glud, N. B. Ramsing, J. K. Gundersen, and I. Klimant, "Planar Optrodes: a New Tool for Fine Scale Measurements of Two-dimensional O_2 Distribution in Benthic Communities," Marine Ecology Progress Series, 140, 217-226, 1996.

[10] G. Holst and B. Grunwald, "Luminescence Lifetime Imaging with Transparent Oxygen Optodes," Sensors and Actuators B: Chemical, 74, 78-90, 2001.

[11] K. R. Castleman, "Concepts in Imaging and Microscopy: Color Image Processing for Microscopy," The Biological Bulletin, 194, 100-107, 1998.

[12] B. E. Bayer, "Color imaging array," U.S. Patent 3 971 065, July 1976.

[13] http://en.wikipedia.org/wiki/Bayer_filter, Bayer Filter, August 2009.

[14] P. Rolfe, "In Vivo Chemical Sensors for Intensive Care Monitoring," Medical and Biological Engineering and Computing, 28, B34-B47, 1990.

[15] P. Yager, Biomedical Sensors and Biosensors, in: B. D. Ratner, A. S. Hoffman, F. J. Schoen, J. E. Lemons (Eds.), Biomaterials Science, Academic Press, 375-388, 1996.

[16] A. P. Demchenko, "The Problem of Self-calibration of Fluorescence Signal in Microscale Sensor Systems," Lab on a Chip, 5, 1210-1223, 2005.

[17] J. Park, C. Kim and Y. Kim, "A Simple On-chip Self-diagnosis/Self-calibration Method of Oxygen Microsensor Using Electrochemically Generated Bubbles," Sensors and Actuators B, 108, 633-638, 2005.

[18] J. Park, C. Kim and M. Choi, "Oxidase-coupled Amperometric Glucose and Lactate Sensors with Integrated Electrochemical Actuation System," IEEE Transactions on Instrumentation and Measurement, 55, 1348-1355, 2006.

[19] T. C. Merkel, V. I. Bondar, K. Nagai, B. D. Freeman and I. Pinnau, "Gas sorption, diffusion, and permeation in poly(dimethylsiloxane)," Journal of Polymer Science: Part B: Polymer Physics, 38, 415-434, 2000.

PAPER

1. Color Intensity Method for Two-Dimensional Oxygen Measurements with an Optical Sensor Array

Abstract

The oxygen imaging technique to obtain a two-dimensional distribution is a convenient method because it does not require individual addressing of each sensing element in a sensor array. Until recently, color charge coupled devices (CCDs) have rarely been used for oxygen imaging in spite of usefulness for analyzing the spectral content of images. In this work, a color CCD camera was used for luminescence intensity imaging, and two methods of color intensity analysis are investigated and compared. The first method is to analyze the total Red-Green-Blue (RGB) color intensity of the original color image. The second method involves extracting the red color element to enhance the sensitivity of oxygen measurement. Both commercial RedEye^{TM} oxygen-sensitive patches and lab-made photopatterned hydrogel sensor arrays were used to verify these methods. The linearity and sensitivity of oxygen detection based on the red intensity analysis was improved to those of spectrometric measurement and total color intensity analysis. This method also has potential applications in lifetime imaging, multi-analyte detection, and simultaneous structural and functional imaging of biological systems.

Keywords

Charge coupled devices, luminescence, imaging, ruthenium

Introduction

Optical oxygen sensors are gradually replacing their electrochemical counterparts because they do not consume oxygen during measurement and do not interfere with

electrical devices. Additionally, optical oxygen sensors are particularly useful in the area of biological oxygen monitoring because of their potential for noninvasive detection and miniaturization.

The measurement and control of a two-dimensional oxygen distribution can provide valuable information in a variety of biological experiments, especially when studying the influence of oxygenation in biological systems and optimizing the growth environment during microbial, cell, and tissue culture [1-4]. The electrochemical method for two-dimensional measurement involves a considerable number of microelectrodes. Meyer et al. arranged 400 platinum microelectrodes onto a $1cm^2$ matrix and mapped two-dimensional oxygen and hydrogen peroxide distribution by sequential reading of each electrode to acquire the spatial and temporal oxygen changes at an implantation site [5]. In contrast to electrochemical detection, most optical oxygen sensors operate on the principle that oxygen quenches the luminescence emitted from luminescent dyes that are immobilized in an oxygen permeable membrane [6]. Luminescence based optical oxygen measurement typically utilizes a spectrometer; however, spectrometers are usually intended for one-dimensional analysis of a small sample area. Unfortunately, both electrochemical measurement and spectrometer-based optical detection are somewhat incompatible with two-dimensional oxygen measurement because simultaneous detection at multiple sites is required.

A better approach for two-dimensional oxygen measurement is to utilize imaging techniques to obtain the oxygen distribution from images of planar optical oxygen sensor foils or arrays. Such oxygen imaging can utilize either luminescence intensity or lifetime measurement [7]. As an example of this, Glud et al. performed two-dimensional oxygen measurement in benthic communities by analyzing the intensity of emission from an oxygen-quenchable fluorophore foil in contact with sediments [8]. Holst et al. measured the oxygen distribution in photosynthetic communities by measuring the decay time of luminescence from planar optical sensor images [9]. Although not focused on oxygen distribution imaging, other examples were also reported. For example, Cho and Bright reported an integrated optical sensor array based on micromachined wells formed directly on an LED face and filled with oxygen sensitive luminophores [10]. Multi-analyte sensor arrays are another type of sensors based on imaging [11-12]. For all these works,

monochrome CCD cameras were used for luminescence imaging with optical filters to narrow down the detection range of the device.

The color CCD camera is a common tool in both bare optical imaging for structural examination and functional imaging for biochemical information extraction. Therefore, color CCD cameras can serve multiple purposes when analyzing biological samples. Until recently, however, color CCDs have rarely been used for imaging oxygen sensor arrays. Part of the problem with using color CCDs is that they are inherently biased towards the detection of green light in order to mimic the human eye. Using a color extraction technique to remove unnecessary color information from an image could overcome this and other limitations. There are interesting colorimetric approaches by a handful of researchers based on absorption or multiple-luminophore methods, although these types of devices appear to provide semi-quantitative results [13-15].

With this background information in mind, a red color analysis method is proposed herein to eliminate unnecessary and distorted information from the color CCD image of a sensor array for enhanced dissolved oxygen measurements. The luminescence quenching of Ru(II)-complexes embedded in poly(ethylene glycol) (PEG) hydrogels was used as the basic detection mechanism for this research [16]. Two-dimensional oxygen sensor arrays were prepared with photopatternable PEG [17] and characterized by a color extraction process.

Experiments

Hydrogel Matrix Photopatterning

Patterning a hydrogel sensor array is possible through the addition of photoinitiator to a PEG-based hydrogel precursor. The resulting hydrogel physically entraps a ruthenium complex. Revzin et al. photopatterned 7 to 600 μm diameter cylinder structures by adding 2,2-dimethoxy-2-phenylacetophenone photoinitiator to PEG [17]. By controlling PEG macromer molecular weight, they varied the height of the structures from 2 to 12 μm. O'Neal et al. also combined a photopatternable PEG matrix with ruthenium complexes to fabricate optical oxygen sensor array [16]. A similar procedure was used for this research, and Dichlorotris(1,10–phenanthroline) ruthenium (II) hydrate (98%, Sigma Aldrich) was the oxygen sensitive fluorescent compound used

for this study. PEG diacrylate (Sigma Aldrich, Mn: 575) was used as the matrix to immobilize the ruthenium complexes. A precursor solution was prepared by dissolving ruthenium (II) complex powder into a mixture of methanol and toluene (4:1, v:v) at a concentration of 5 mg/ml. The resulting solution (2% v/v) was thoroughly mixed with PEG diacrylate (60%, v/v), photoinitiator (Darocur 1173, Ciba, 2% v/v), and deionized water (36% v/v).

Oxygen Sensor Assembly

The fabrication steps for the array are illustrated in Figure 1. The prepared oxygen sensor precursor solution was injected with a syringe into a fluidic chamber which consisted of two slide glass (1" x 3"), PTFE (polytetrafluoroethylene) spacer (STE-0005-D, 0.005'' thick, Small Parts, Inc.), and scotch tape film (3M, 3850 Series). After injecting the precursor solution, the mask was aligned and exposed to UV light at an energy dose of 55 mJ/cm^2 (5.5 mW/cm^2 at 365 nm for 10 seconds). The PTFE spacer, scotch tape film, and lower slide glass were removed after UV exposure, and unpolymerized precursor solution was washed out with running deionized water for 1 minute. After a photopatterning, a silicone CoverWell^{TM} sheet (PC1L-0.5, 32 x 19 x 0.5 mm, Grace Bio-Labs) was placed on top of the slide glass to define the fluidic chamber. The polycarbonate cover (0.18 mm thick), a part of the CoverWell^{TM} product, served as an upper cover layer for the fluidic system. Provided access holes in the polycarbonate film were used as sample inlets and outlets. The finished oxygen sensor assembly was filled with deionized water to prevent the dehydration of the hydrogel array and to remove any residual unpolymerized precursor solution.

To verify the measurement results using the fabricated PEG sensor arrays, a commercial oxygen-sensitive patch (RedEye^{TM}, RE-FOX-8, 8 mm diameter, Ocean Optics) was used as a reference for the same spectrometric and image analysis methods (described later). The RedEye^{TM} contains a ruthenium complex immobilized in a sol-gel matrix. The same fluidic configuration for the PEG sensor array was used for the RedEye^{TM} oxygen-sensitive patch. The patch was attached onto a polycarbonate film surface using the provided adhesive layer of the patch product in place of the PEG array.
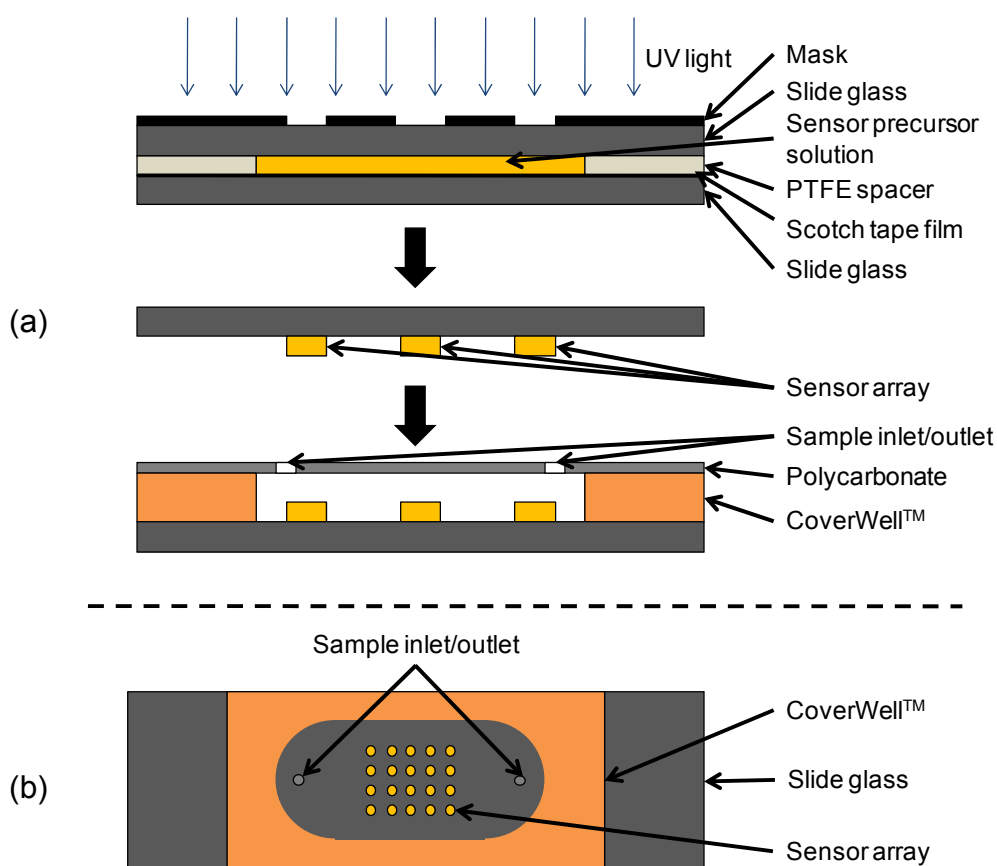
Figure 1. Optical dissolved oxygen sensor assembly. (a) photopatterning of PEG hydrogel sensor array and (b) layout (topview) of the fabricated system. The commercial RedEye[TM] oxygen-sensitive patch was also incorporated in the same assembly structure to replace the PEG array.

Measurement Setup

Two different luminescence intensity measurements were performed. Figure 2 (a) shows the fluorescence imaging system for the fabricated oxygen sensor assembly. A blue LED (NSPB500S, peak wavelength 470 nm typ., Nichia) was used as the excitation source for the immobilized ruthenium complexes, and a color CCD camera (DS-5M, 5-megapixel, Bayer-masked, Nikon) was used for image capturing. A long-wave pass filter (10LWF-500-B, cut-on wavelength 500 nm, Newport) was used at the receiving end to eliminate the intense blue wavelength range. To verify the proposed image analysis method, results were compared with those of spectrometric measurements under the same conditions as in Figure 2 (b). A spectrofluorometer (USB2000-FLG, Ocean Optics) was used as the detector. A blue LED light source (LS450, output wavelength 470 nm, Ocean Optics) was used as the excitation source. A reflection probe (R400-7-UV-VIS, Ocean

Optics), consisting of six illumination fibers (400 μm diameter each) and one read fiber (400 μm diameter) was used to capture luminescence from the samples. A black sheet was placed under the sensor assembly and all measurements were done in dark environment. For both methods, the concentration of oxygen was regulated by bubbling different ratios of O_2 and N_2 gases into deionized water with mass flow controllers. Once the water was saturated to a specific level, it was injected into the fabricated sensor assembly with a syringe pump.
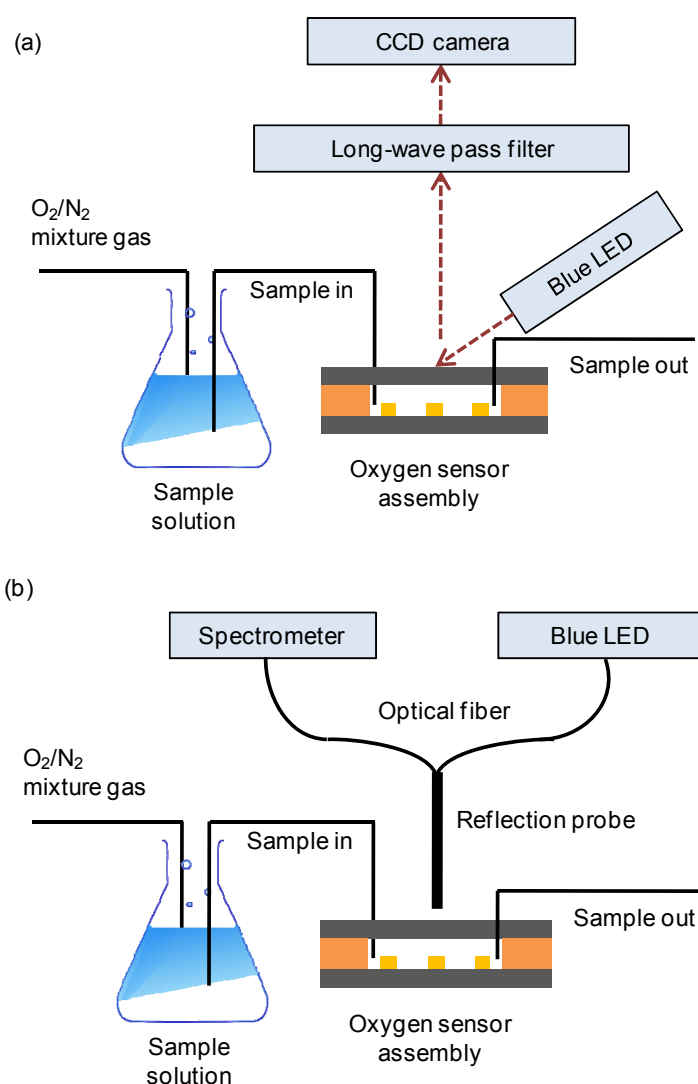
Figure 2. Two measurement setups. (a) sensor array imaging with a CCD camera and a long-wave pass filter (cut-on wavelength 500 nm) and (b) single sensor spectral analysis with a spectrometer without the filter.

Sensor Image Analysis

Figure 3 (a) shows the original color image of RedEye^{TM} oxygen-sensitive patch in 0% oxygen saturated water. There are two different points of view to extract oxygen related information: the wavelength domain and the color space domain. Since colors are represented by the combination of red (R), green (G), and blue (B) elemental components in the RGB color model, three-dimensional vector coordination can be used to describe colors. Each pixel within a region of interest (ROI), (indicated with a white dashed line in Fig 3 (a)) can be represented in Euclidean space (as in Figure 3 (b)) using ImageJ software [18]. The emission spectra of the RedEye^{TM} oxygen-sensitive patch taken in 0, 10, 20, 40, 60, 80, and 100% oxygen saturated water are shown in Figure 3 (c). The peak emission wavelength is at 595 nm, which corresponds to an orange color between yellow (570-580 nm) and red (625-740 nm). The oxygen-dependent emission lies within a wide range of 550-750 nm with most of it falling in the range of colors in which the red element is dominant (i.e., orange - red). This implies that the red color element is the significantly more relevant to oxygen than the blue and green elements in the color space domain.

Until recently, the luminescence imaging of oxygen sensors was primarily conducted with monochrome CCD cameras [8-12]. From a color space perspective, this introduces a considerable amount of unnecessary blue and green elements. In some cases, band-pass filters were used to narrow down the range of interest. Unfortunately, this may lead to a loss of emission in the rest of the oxygen-related range of 550-750 nm. Therefore, the most efficient way to selectively harvest oxygen information is the color space domain approach by extracting only red color from the original image, rather than by the wavelength domain approach using filters. With this in mind, two methods of oxygen measurement were investigated: total color intensity method and red intensity method which are outlined below.

The first method was to analyze the total color intensity of the original RGB color image to translate this into oxygen concentration. This approach is essentially the same concept as previous oxygen imaging methods except that the images were taken with a color CCD instead of the monochrome CCD. Here, the total color intensity of a pixel is represented by the magnitude of its vector (i.e., square root of $R^2+G^2+B^2$). Consequently,

each pixel in the color space assumes a value in the range between 0 and 255 (arbitrary unit after 8-bit processing). Therefore, a change in total color intensity derived from the change of RGB vector magnitude includes unnecessary information that is not related to the change in oxygen concentration (i.e., G and B components).
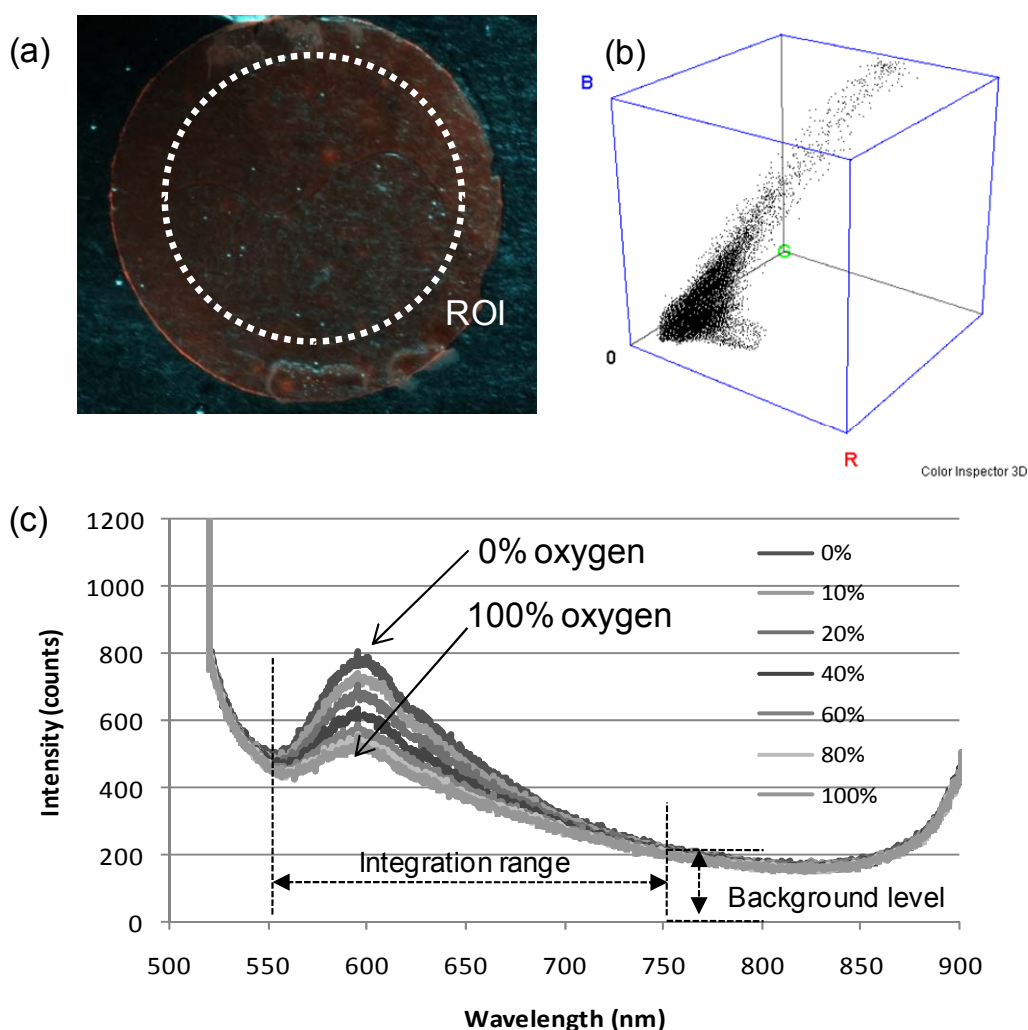
Figure 3. Three different representations of a commercial RedEye[TM], oxygen-sensitive patch (8 mm diameter). (a) original color image at 0% oxygen saturated water obtained with a color CCD and a long-wave pass filter (cut-on wavelength 500 nm), (b) RGB vector distribution of Figure 3 (a) (0% oxygen saturated water) for every pixel within the region of interest (ROI), and (c) spectra in 0, 10, 20, 40, 60, 80, and 100% oxygen saturated water measured with a spectrometer without long-pass filter, which leaves a large peak (below 525 nm) from the blue LED source.

The second method involves extracting only the red vector components to enhance the sensitivity of oxygen measurement. The red color extraction serves as a virtual band-pass filter by removing unnecessary information not related with oxygen from the original image. This virtual band-pass filter also has the added benefit of overcoming the inherent color distortion of the CCD camera. It should be noted that the color CCD intentionally distorts the natural color intensity in order to adapt it to the human eye, which is more sensitive to green than red or blue [19]. Most CCDs accomplish this by utilizing Bayer masks over the CCD surface to split red, blue, and green colors spatially [20]. Each pixel element is composed of four sub-pixels: one sub-pixel receives red, one receives blue, and the other two sub-pixels detect green intensity to obtain all the color information for the pixel. This means that the CCD camera is more sensitive to green because it has more pixel elements for green color detection. The red color extraction procedure utilized in this work is capable of overcoming the enhanced green color band that is inherent in color CCD imaging.

Figure 4 (a) and (b) show projected pixel distributions on the red-green (R-G) plane in 0% and 100% oxygen saturated water, respectively. As seen in Figure 4 (c) and (d), red vector intensities of all pixels in the image are projected onto the red axis by the red color extraction process and the histograms show the distribution of intensities between 0 and 255 (arbitrary unit). The changes in intensity distribution projected on the red axis are more directly relevant to the change of oxygen concentration than those on the green or blue axes. The change in mean intensity values represents the change of oxygen concentration. For both total color and red color analysis methods, procedures for object extraction and intensity calculation are required. The Otsu's thresholding method was chosen among many available segmentation techniques because of its well-separated distributions between objects and the background in the images of the oxygen sensor array taken in this study [21-22].

Results and Discussion

Spectrometry and Color Intensity Methods Using RedEye[TM] Oxygen-Sensitive Patch

The spectrum of the RedEye[TM] oxygen-sensitive patch was first analyzed with the reflection probe and spectrometer. Only a part of the oxygen patch area was analyzed because of the relatively small active area of the reflection probe (400 μm diameter) compared with the patch (8 mm diameter). As shown in Figure 3 (c), the emission peak is at 595 nm for every case and peak intensity drops with increasing oxygen concentration, as expected. After this initial test with a spectrometer, the analysis of total color intensity and red color intensity of RedEye[TM] was performed. Figure 5 (a) is the histogram of total color intensity distribution in the patch, based on the color space vectors (shown in Figure 3 (b)) in 0, 20, and 100% oxygen saturated water. Figure 5 (b) shows the red-extracted images after the red color extraction procedure from the original images and Figure 5 (c) shows a red color histogram at the same conditions. The mean value of the intensity distribution decreases due to oxygen quenching as the dissolved oxygen concentration in the sample increases in both cases in Figure 5 (a) and (c). The normalized intensities (i.e., $I(0)/I$) of all three methods are plotted in Figure 6 according to the following Stern-Volmer equation:

$$I(0)/I = 1 + K_{SV} C \tag{1}$$

where $I(0)$ and I represent the intensities in the absence and presence of oxygen respectively, K_{SV} is the quenching constant, and C is the oxygen concentration. This is the most common way of presenting optical oxygen sensor performance [23]. For the spectrometer, these are the intensities at the peak wavelength (595 nm) of Figure 3 (c). The spectrum integration (i.e., the area under each spectrum) was also performed over the wavelength range from 550 nm to 750 nm, but the constant background noise level (i.e., minimum intensity 196 at 750 nm) was subtracted for the calculation as shown in Figure 3 (c). For the image analysis methods, they represent the mean values of total color (RGB) vector magnitudes and the red-projected color vector magnitudes for the total color analysis and the red color analysis, respectively (shown in Figure 5 (a) and (c)).

Additionally, the curves using green color analysis and spectrum integration are also shown. The linearity and sensitivity of oxygen detection based on red intensity analysis are superior to those of spectrometric measurements and total intensity analysis.
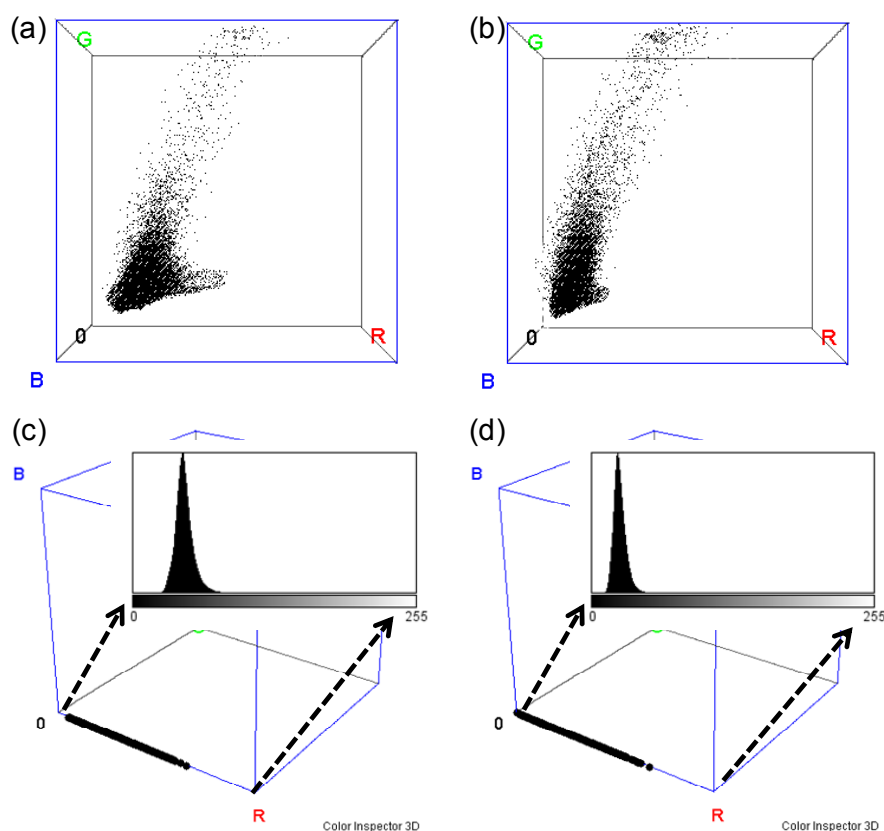
Figure 4. Red color extraction procedure represented with ImageJ software: (a) projection of RGB vectors onto G-R plane (0% oxygen saturated water), (b) projection of RGB vectors onto G-R plane (100% oxygen saturated water), (c) histogram of red intensity distribution (0% oxygen saturated water), and (d) histogram of red intensity distribution (100% oxygen saturated water). Vertical axes are normalized counts in the histograms.

It is reasonable to expect that the sensitivity based on the red intensity is higher than that of the total intensity. This is because the total intensity obtained by a color CCD includes an enhanced green element that has little relevance to oxygen, as explained earlier. This fact is apparent from the lowest sensitivity of the curve obtained by green color analysis in Figure 6. The red color extraction eliminates this green element from the original color image to obtain the oxygen concentration more effectively.

The parameter used in the spectrometric curve is the intensity value at a specific wavelength of 595 nm. In fact, this peak intensity reading can be considered as a case of using an extremely narrow band-pass filter. In contrast, the red intensities in the red color analysis include all oxygen-specific information extracted from the wide range of fluorescence emission. Therefore, the red color analysis method exhibits a superior sensitivity to the spectrometry analysis based on a specific wavelength. However, a higher sensitivity closer to that of the red intensity method was obtained by the spectral integration that is considered to be analogous with the "red intensity method" in the wavelength domain.

The red intensity method is expected to be more efficient if it is applied to oxygen sensitive porphyrin (PtOEP) luminophore because its emission wavelength is more reddish than that of ruthenium complexes [15]. This method is also anticipated to produce better results for luminescence lifetime imaging. Because of these results using the RedEye[TM] oxygen-sensitive patch, the red color analysis method was chosen for characterizing the two-dimensional oxygen PEG array.

Photopatterned PEG Array

Ruthenium complexes were immobilized in the PEG matrix and patterned on a slide glass and a fluidic system was prepared as described previously. In total, 20 sensor spots were photopatterned into a 4x5 matrix within a 1 cm^2 area. In this proof-of-concept stage, the sensor was designed to be rather large. Each sensor spot was 500 μm in diameter and 120 μm in height when in a swollen state. Some of the sensor spots were washed away after pattern development due to insufficient adhesion to the bare glass surface. Adhesion was improved by silanization of the glass slide surface. A small amount of 1-wt.% 3-aminopropyltriethoxysilane (3-APTES, Sigma Aldrich) was applied onto the glass slide surface and cured for 30 min at 80 ∘C for surface silanization before injecting the sensor precursor solution. A scotch tape film was used to prevent the sensor array from being attached to the lower slide glass and was removed after sensor patterning as illustrated in Figure 1.
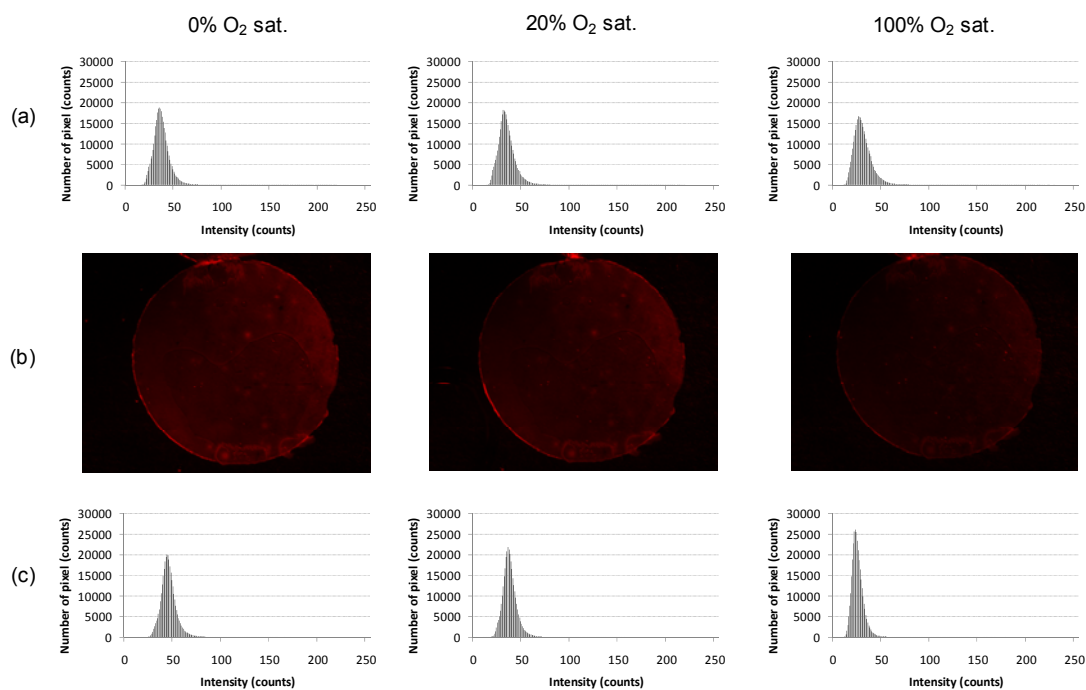
Figure 5. Color intensity analysis of the RedEye[TM] oxygen-sensitive patch images in 0, 20, and 100% oxygen saturated water. (a) Histograms based on total color (RGB) intensity analysis, (b) red-extracted images of the RedEye[TM] oxygen-sensitive patch (8 mm diameter), and (c) histograms based on red color (R) intensity analysis.
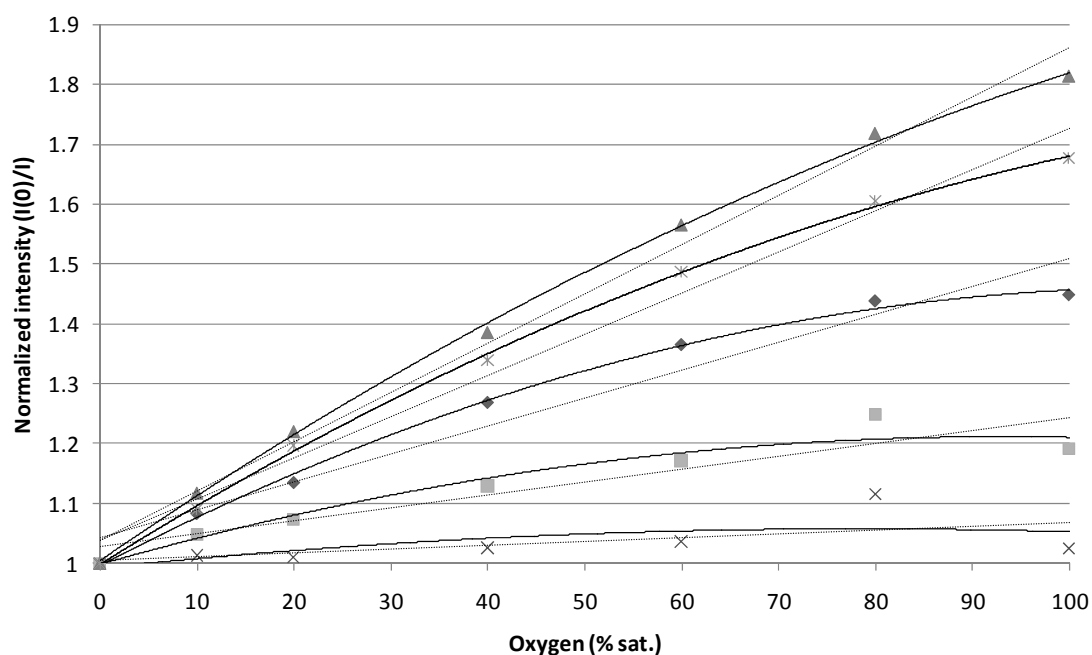
	Linear trendline	Polynomial trendline
Red intensity (▲)	y = 0.0082x + 1.0386 R² = 0.9897	y = -3E-05x² + 0.0111x + 1.0033 R² = 0.9990
Spectrum integration(*)	y = 0.0069x + 1.0372 R² = 0.9828	y = -3E-05x² + 0.0101x + 0.998 R² = 0.9992
Spectrometry at 595 nm (♦)	y = 0.0047x + 1.0416 R² = 0.9510	y = -4E-05x² + 0.0084x + 0.996 R² = 0.9974
Total color intensity (■)	y = 0.0022x + 1.0266 R² = 0.8655	y = -2E-05x² + 0.0046x + 0.9972 R² = 0.9471
Green intensity (x)	y = 0.0006x + 1.0044 R² = 0.3705	y = -1E-05x² + 0.0017x + 0.9917 R² = 0.4496

Figure 6. Stern-Volmer plots with respect to dissolved oxygen based on red color (R) intensity, spectrometry (595 nm), spectrum integration (550-750 nm) after background noise subtraction, total color (RGB) intensity, and green color (G) intensity.

Spectrometry and Red Color Analysis Method Using Photopatterned PEG Array

Figure 7 shows the typical emission spectra of sensor spots in 0, 10, 20, 40, 60, 80, and 100% oxygen saturated water. The spectra has a similar shape and the same peak emission wavelength as the RedEye[TM] oxygen-sensitive patch, which implies that ruthenium emission wavelength is not affected by immobilization in the PEG matrix as in a previous report [16]. Right after the measurement using the spectrometer, the CCD

image was taken for analysis of red color intensity. Figure 8 (a) is the red-extracted images of two-dimensional oxygen sensor array in 0, 20, and 100% oxygen saturated water. Figure 8 (b) and (c) shows corresponding pixel distributions of the original total color images in RGB vector space and red color histograms, respectively. The mean value of red color intensity decreases with respect to the dissolved oxygen concentration of the sample due to the quenching. The averaged I(0)/I values of 20 sensor spots are plotted in Figure 9 (a) to compare with those obtained with the spectrometer. The sensitivity and linearity of the red color intensity show a significant improvement over those of the spectrometer curve because of the same reasons as described in the discussion of the RedEye[TM] oxygen-sensitive patch.

Figure 9 (c) shows three-dimensional surface plots of total color intensities of the two-dimensional array of Figure 8 (a) in 0 and 100% oxygen saturated water using ImageJ software. As can be seen in the plot, the absolute intensities of the sensor spots at a certain oxygen concentration are not spatially even because of inhomogeneous illumination intensity of the blue light over the sensor array. Furthermore, although all sensors were prepared by a single batch process, each sensor may have different sensitivities (I(0)/I) and zero-oxygen intensities (I(0)) due to the possible variation of PEG thickness and uneven distribution of ruthenium complex concentration. After a "one-shot" image analysis, however, the sensitivities of each sensor can be simultaneously plotted as in Figure 9 (b). This is, of course, the inherent advantage of the image analysis method because it allows for the calibration of multiple sensors simultaneously for two-dimensional mapping.

Viewed from an object segmentation standpoint, the red-extracted image has another advantage over the original image. The object regions (i.e., sensor spots) are separated much more easily in the red-extracted image by a very common and simple segmentation technique such as Otsu's thresholding method because the residual blue excitation light can be filtered out after the red-extraction process. Figure 9 (d) shows surface plots of red intensities of Figure 8 (a) in 0 and 100% oxygen saturated water. Compared with the total intensity surface plot in Figure 9 (d), the signal-to-noise ratio of the array intensity is dramatically improved and noise spikes are effectively suppressed.

This feature of red color analysis for oxygen measurement is suitable for fast and automatic ROI selection for the image process.

There are many other unique features of this kind of photopatterned optical sensor array. It allows for optical observation of biological samples through locally transparent windows not occupied by the sensor spots. Simultaneous two-dimensional chemical mapping and optical observation can be accomplished by simply switching between a wide-band light source and a blue source. In this study, a long-wave pass filter was used to screen out the very strong blue excitation wavelength range. However, with the proper choice of a wide-band light source that allows for both oxygen sensor excitation and illumination for bare structural imaging, it is expected that this filter could be eliminated. The photopatterned array can also be adopted for simultaneous multi-analyte determination using multiple sensor arrays (including pH and possibly other ions with different luminophores) [11-12].
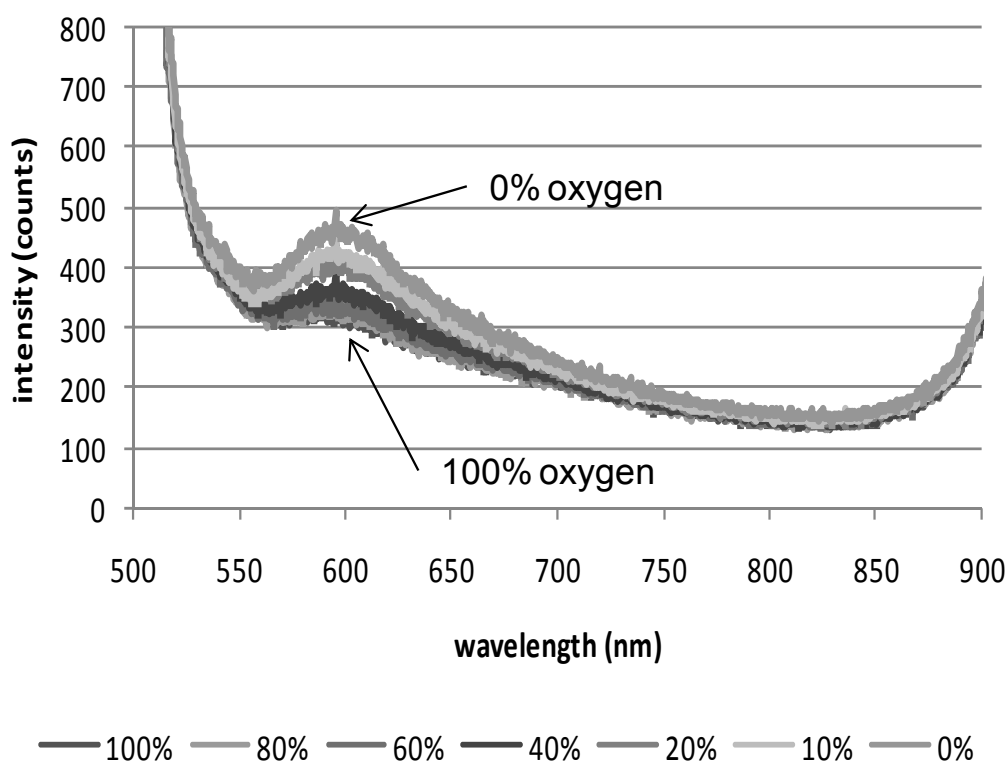
Figure 7. Spectra of PEG dissolved oxygen sensor array taken in 0, 10, 20, 40, 60, 80, and 100% oxygen saturated water.
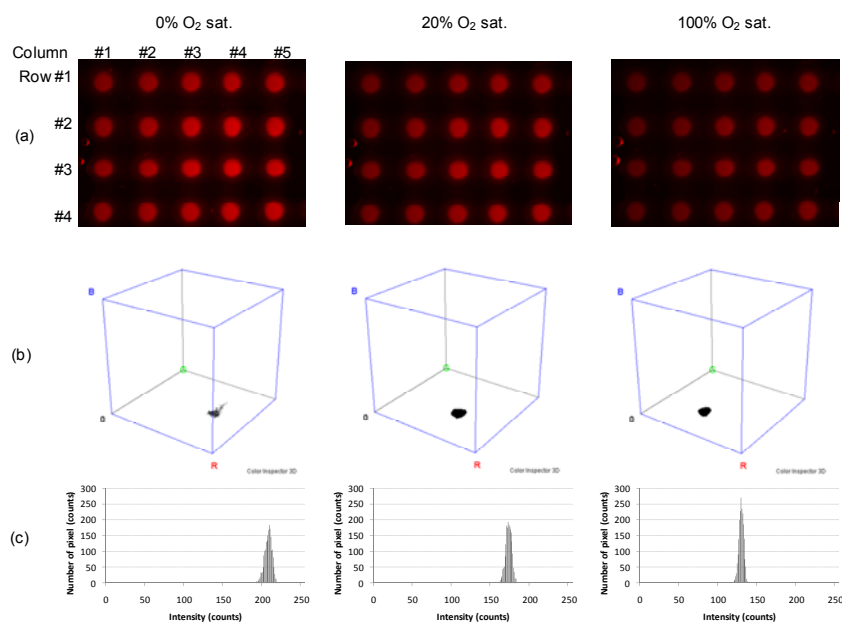
Figure 8. Color intensity analysis of PEG dissolved oxygen sensor array in 0, 20, and 100% oxygen saturated water. (a) Red-extracted images, (b) pixel distributions of one sensor spot in RGB vector space, and (c) histograms of a sensor spot based on the red color analysis method.
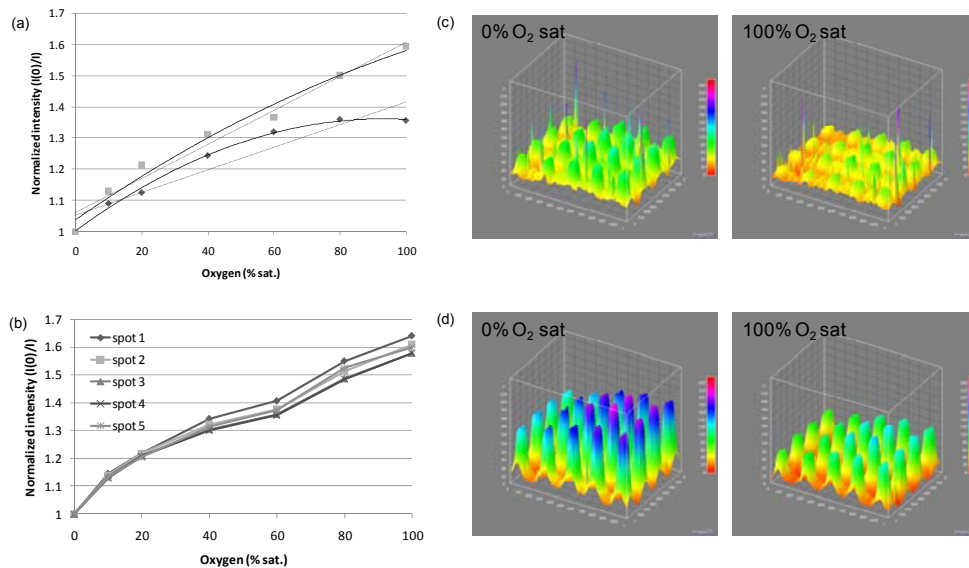
Figure 9. Responses of PEG dissolved oxygen sensor array. (a) Stern-Volmer plots with respect to dissolved oxygen based on spectrum and red color analysis (red intensity plot shows averaged values of 20 spots.), (b) normalized intensities of row #3 sensor spots at various oxygen concentrations, (c) surface plot of total color intensities of array in 0 and 100% oxygen saturated water, and (d) surface plot of red intensities of array in 0 and 100% oxygen saturated water.

Conclusion

Photopatterned PEG hydrogel arrays with embedded Ru-complexs were used as oxygen detection platform in this research. It was demonstrated that the red intensity analysis method with a color CCD showed improved linearity and sensitivity over spectrometry and total color intensity methods by effectively extracting oxygen-related color information. In addition to its performance improvement, the sensor array with the red intensity method offers many other prospective advantages. It allows calibrating multiple sensors in an array simultaneously for two-dimensional mapping. The red intensity method can be adapted to other optical sensors using different luminorphores or to luminescence lifetime measurements. Moreover, the proposed technique is expected to serve multiple purposes simultaneously such as bare optical imaging and functional imaging when analyzing biological samples.

References

[1]   W. W. Minuth and R. Strehl, "Technical and theoretical considerations about gradient perfusion culture for epithelia used in tissue engineering, biomaterial testing and pharmaceutical research," Biomedical Materials, vol. 2, pp. R1-R11, 2007.

[2]   Y. Martin and P. Vermette, "Bioreactors for tissue mass culture: Design, characterization, and recent advances," Biomaterials, vol. 26, pp. 7481-7503, 2005.

[3]   J. Malda, J. Rouwkema, D. E. Martens, E. P. le Comte, K. Y. Kooy, J. Tramper, C. A. van Blitterswijk, and J. Riesle, "Oxygen gradients in tissue-engineered Pegt/Pbt cartilaginous constructs: Measurement and modeling," Biotechnology and Bioengineering, vol. 86, pp. 9-18, 2004.

[4]   J. Park, T. Bansal, M. Pinelis, and M. M. Maharbiz, "A microsystem for sensing and patterning oxidative microgradients during cell culture," Lab on a Chip, vol. 6, pp. 611-622, 2006.

[5] H. Meyer, H. Drewer, B. Grundig, and K. Cammann, "Two-dimensional imaging of O2, H2O2, and glucose distributions by an array of 400 individually addressable microelectrodes," Analytical Chemistry, vol. 67, pp. 1164-1170, 1995.

[6] O. S. Wolfbeis, "Materials for fluorescence-based optical chemical sensors," Journal of Materials Chemistry, vol. 15, pp. 2657-2669, 2005.

[7] M. Kühl and L. Polerecky, "Functional and structural imaging of phototrophic microbial communities and symbioses," Aquatic Microbial Ecology, vol. 53, pp. 99-118, 2008.

[8] R. N. Glud, N. B. Ramsing, J. K. Gundersen, and I. Klimant, "Planar optrodes: a new tool for fine scale measurements of two-dimensional O2 distribution in benthic communities," Marine Ecology Progress Series, Vol. 140, pp. 217-226, 1996.

[9] G. Holst and B. Grunwald, "Luminescence lifetime imaging with transparent oxygen optodes," Sensors and Actuators B: Chemical, vol. 74, pp. 78-90, 2001.

[10] E. Cho and F. V. Bright, "Optical sensor array and integrated light source," Analytical Chemistry, vol. 73, pp. 3289-3293, 2001.

[11] S. Lee, B. L. Ibey, G. L. Coté, and M. V. Pishko, "Measurement of pH and dissolved oxygen within cell culture media using a hydrogel microarray sensor," Sensors and Actuators B: Chemical, vol. 128, pp. 388-398, 2008.

[12] G. Liebsch, I. Klimant, B. Frank, G. Holst, and O. S. Wolfbeis, "Luminescence lifetime imaging of oxygen, pH, and carbon dioxide distribution using optical sensors," Applied Spectroscopy, vol. 54, pp. 548-559.

[13] K. Eaton, "A novel colorimetric oxygen sensor: dye redox chemistry in a thin polymer film," Sensors and Actuators B: Chemical, vol. 85, pp. 42-51, 2002.

[14] R. C. Evans, P. Douglas, J. A. G. Williams, and D. L. Rochester, "A novel luminescence-based colorimetric oxygen sensor with a "traffic light" response," Journal of Fluorescence, vol. 15, pp. 201-206, 2006.

[15] R. C. Evans and P. Douglas, "Controlling the color space response of colorimetric luminescence oxygen sensors," Analytical Chemistry, vol. 78, pp. 5645-5652, 2006.

[16] D. P. O'Neal, M. A. Meledeo, J. R. Davis, B. L. Ibey, V. A. Gant, M. V. Pishko and G. L. Coté, "Oxygen sensor based on the fluorescence quenching of a ruthenium complex immobilized in a biocompatible poly(ethylene glycol) hydrogel," IEEE Sensors Journal, vol. 4, pp. 728 – 734, 2004.

[17] A. Revzin, R. J. Russell, V. K. Yadavalli, W. Koh, C. Deister, D. D. Hile, M. B. Mellott, and M. V. Pishko, "Fabrication of poly(ethylene glycol) hydrogel microstructures using photolithography," Langmuir, vol. 17, pp. 5440-5447, 2001.

[18] M. D. Abramoff, P. J. Magelhaes, and S. J. Ram, "Image processing with ImageJ," Biophotonics International, vol. 11, pp. 36-42, 2004.

[19] K. R. Castleman, "Concepts in imaging and microscopy: color image processing for microscopy," The Biological Bulletin, vol. 194, pp. 100-107, 1998.

[20] B. E. Bayer, "Color imaging array," U.S. Patent 3 971 065, July 1976.

[21] R. M. Haralick and L. G. Shapiro, "Image segmentation techniques," Computer Vision, Graphics, and Image Processing, vol. 29, pp. 100-132, 1985.

[22] R. C. Gonzalez and R. E. Woods, Digital image processing. Upper Saddle River, NJ: Prentice Hall, 2002, ch. 10.

[23] J. R. Bacon and J. N. Demas, "Determination of oxygen concentrations by luminescence quenching of a polymer-immobilized transition-metal complex," Analytical Chemistry, vol. 59, pp. 2780-2785, 1987.

2. A simple Quantitative Chemical Imaging Method with Broad-Band Light Source and Color CCD

Abstract

Simultaneous acquisition of chemical information during structural observation is highly advantageous in analyzing biochemical or biological samples. It combines the merits of digital imaging with the attributes of spectroscopic measurements. Functional chemical imaging for this purpose, however, mostly requires special light sources and optical filters compared to simple structure observation. For example, fluorescent optical oxygen measurement requires a blue light source for excitation of the optical sensor (e.g., ruthenium complex) and a long-wave pass filter at the photodetector to eliminate the strong excitation light (e.g., blue wavelength) from the acquired image. In this research, a simple color analysis method was employed to eliminate the use of filter and replace the blue light source with a broad-band white light-emitting diode (LED). Commercial RedEye[TM] oxygen-sensitive patches were used to verify this method. All images were taken with a color charge coupled device (CCD) camera and the influence of factors for image acquisition such as light source, optical filter, and color analysis method were evaluated in terms of sensitivity for quantitative oxygen imaging. Even without using the blue light source and filter, a good sensitivity to oxygen was obtained with the simple red color analysis method. This simple, new method has potential applications in multi-analyte monitoring and simultaneous structural/functional imaging of biological samples with a general broad-band light source.

Keywords

Functional imaging, luminescence, oxygen, ruthenium

1. Introduction

Electronic color imaging devices such as charge-coupled device (CCD) and complementary metal-oxide-semiconductor (CMOS) is a useful tool for quantitative chemical measurement. Since the CCD or CMOS image sensors can detect variation of optical properties (e.g., intensity change) over multiple positions represented by pixels, it is possible to accomplish instantaneous two-dimensional chemical mapping in a sample.

One of the most benefited areas from this emerging imaging method is the field of aquatic microbial ecology and biogeochemistry [1]. Optical sensor foils (i.e., planar optodes) are used for mapping oxygen [1-7], carbon dioxide [7], and pH [7-9] distribution. These chemical measurements with planar sensors typically utilize optical indicator dyes which are immobilized in thin film matrices and their optical properties such as luminescence and absorbance are detected.

However, quantitative chemical imaging needs additional optical filters and light sources depending on the sensor excitation and emission wavelengths. For example, ruthenium-based fluorescence measurement for optical oxygen detection requires optical filters at the light source and/or photodetector to enhance the sensitivity. The requirement of these optical components for functional chemical imaging makes it difficult to implement truly simultaneous structural observation and functional imaging. A new chemical imaging technique will enable us to use the same optical setting for both purposes.

A simple color analysis method and a color CCD camera were employed to eliminate the need of an optical filter and replace the blue light source with a general broad-band white light-emitting diode (LED) in oxygen quantification. Commercial oxygen-sensitive patches were used to verify this method. The influence of factors for image acquisition such as light source, optical filter, and color analysis method were evaluated in terms of sensitivity for quantitative oxygen imaging.

2. Materials and Methods

2.1 Optical Oxygen Sensor

Commercially available oxygen-sensitive patch (RedEye[TM], RE-FOX-8, 8 mm diameter, Ocean Optics) was used as an optical oxygen sensor in this research. It consists of a sensor coating formulation trapped in a sol-gel matrix. The detection mechanism is fluorescence quenching of ruthenium complex to measure the concentration of dissolved oxygen or gaseous oxygen. Light from the excitation source passes through the matrix and excites the sensor coating formulation to emit fluorescence. If the ruthenium complex encounters an oxygen molecule, the excess energy is transferred to the oxygen molecule in a non-radiative transfer, decreasing or quenching the fluorescence emission. The degree of quenching correlates to the concentration of oxygen in the sol-gel matrix, which is in dynamic equilibrium with oxygen in the sample. Fluorescence is collected by the photodetectors such as spectrometer or camera. The fluorescence intensity is measured and related to the concentration of oxygen through the Stern-Volmer equation that is the most common way of presenting optical oxygen sensor performance [10].:

$$I(0) / I = 1 + K_{SV}C \tag{1}$$

where $I(0)$ and I represent the intensities in the absence and presence of oxygen respectively, K_{SV} is the quenching constant, and C is the oxygen concentration.

2.2 Imaging Setup and Analysis

Figure 1 shows the fluorescence imaging system using the RedEye[TM] oxygen-sensitive patch. A blue LED (NSPB500S, peak wavelength 470 nm, Nichia) or a white LED (LS450 with LED-WHITE bulb, 450~630 nm wavelength, Ocean Optics) was used as the excitation source for the immobilized ruthenium complex. A color camera (DS-5M, 5-megapixel, Bayer-masked, Nikon) that employs a CCD (ICX282AQ, Sony) was used for image capturing. When the optical filter was needed, a long-wave pass filter (10LWF-500-B, cut-on wavelength 500 nm, Newport) was used at the front of the microscope to eliminate the intense blue wavelength range from the sensor images. The camera exposure time was 5 seconds for the blue excitation without filter and 12 seconds for the

blue excitation with filter and white excitation without filter. A black sheet was placed under the sensor assembly to eliminate possible scattering and reflection and all measurements were done in dark environment. Oxygen percentage of the gas sample was regulated by using mass flow controllers. The sample gas was delivered onto the oxygen-sensitive patch with an incident angle of 40° through a glass tube (1 mm outlet diameter) with a moderate flow rate of 2 liter/min to uniformly deliver the gas over the patch.

The intensities of total color and red color of oxygen sensor images were analyzed by a freeware ImageJ [11]. Figure 2 shows a brief procedure of the color analysis. The total color analysis is to translate the total color intensity of the original RGB color image into oxygen concentration. The red color analysis involves extracting only the red color component to enhance the sensitivity of oxygen measurement. The white dashed lines in Figure 2 show region of interests (ROIs) for the total color and red color analysis and the mean intensities of these ROIs were related with the oxygen concentration in sample.
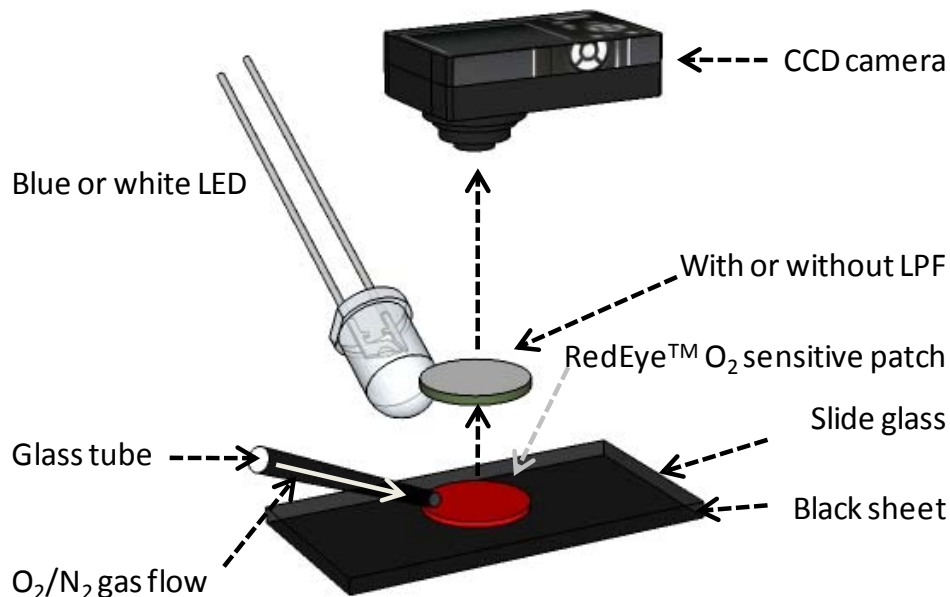
Figure 1. The sensor imaging setup with a color CCD camera. A long-wave pass filter (LPF, cut-on wavelength 500 nm), blue LED (peak wavelength 470 nm), and white LED (450~630 nm wavelength) were selectively used for each experiment of this research. The microscope setup is not shown.
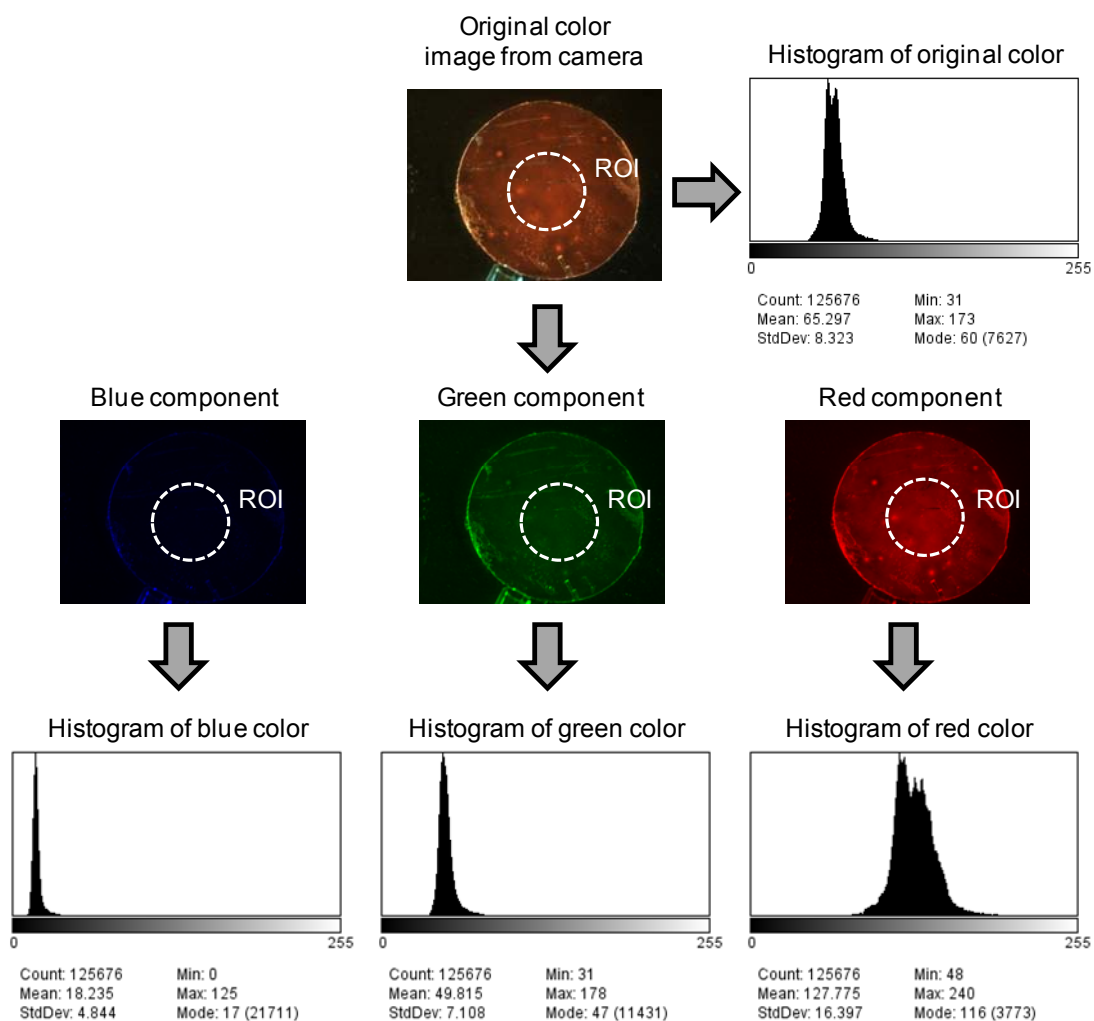
Figure 2. The color analysis procedure for oxygen imaging. A freeware ImageJ program was used for all color processing within the region of interest (ROI).

3. Results and Discussion

3.1 Sensor Image Analysis

Four different series of experiments were performed for gaseous oxygen imaging using a color CCD camera: (1) blue excitation with long-wave pass filter, (2) blue excitation without long-wave pass filter (3) white excitation without long-wave pass filter and (4) comparison between blue and white excitation with an oxygen gradient condition. The purpose of the first two series of measurements was to compare the effectiveness of the filter, while the third one was for evaluating the usefulness of the broad-band white excitation source in quantitative oxygen imaging. The last experiment was for the

performance comparison between blue and white excitation to profile the oxygen gradient in the sample.

The oxygen-related emission from the RedEye[TM] has a peak wavelength at 595 nm and spans in the range of 550-700 nm as in Figure 3 (a). Figure 3 (b) shows the spectral sensitivity characteristics of the CCD chip of the digital camera used for measurement [12]. In the total color analysis method, all spectra detected by the CCD were taken into account to estimate the oxygen content. It should be noted that the oxygen related emission range is almost identical with the response range of red pixels of CCD. Therefore, only the red color spectral sensitivity in Figure 3 (b) remained after the red color extraction process and the CCD signal from other wavelength can be effectively eliminated for oxygen imaging.

Figure 4 shows the original color (i.e., red-green-blue (RGB) total color) and red-extracted images of the oxygen sensor under blue and white excitations with and without the optical filter. The glass tube for the sample gas delivery is shown at the lower right corner of the picture. In all cases, "noise" colors of the short wavelength range (i.e., green~blue color range) that are not related with oxygen change were significantly reduced after the red color extraction process. This effect is much pronounced in the pictures of the sensor configured without the long-wave pass filter, which, in turn, leads to the increase of oxygen sensitivity. The red color extraction serves as a virtual band-pass filter by removing unnecessary information not related with the change in oxygen concentration from the original image. This virtual filter also has an additional benefit of overcoming the inherent color distortion of the CCD camera, which is more sensitive to green than red or blue [13].
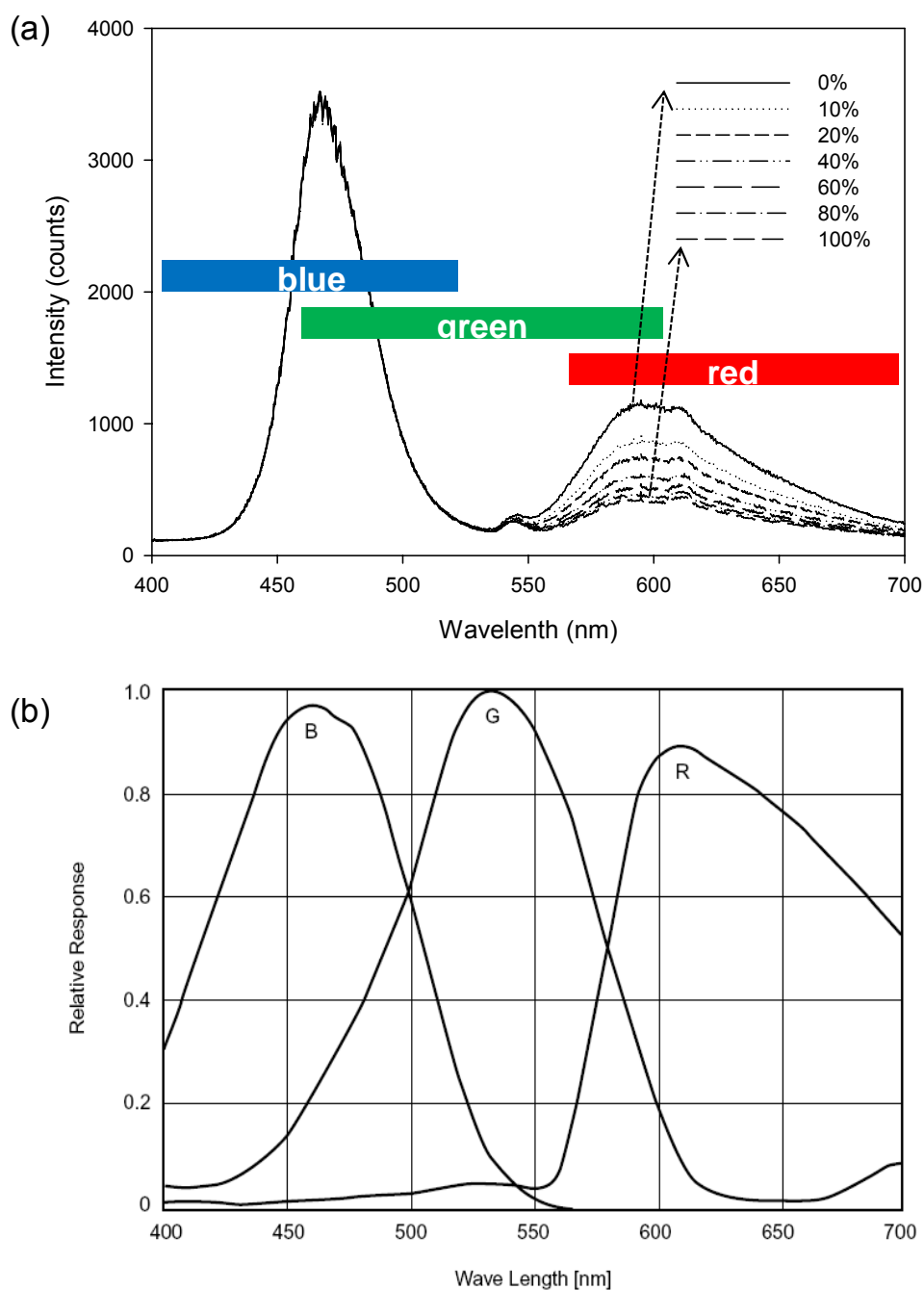
Figure 3. Spectra of RedEye[TM] oxygen-sensitive patch and spectral sensitivity of CCD. (a) Spectra of RedEye[TM] taken at 0, 10, 20, 40, 60, 80, and 100% gaseous oxygen concentration obtained with a spectrophotometer and (b) spectral sensitivity characteristics of CCD (ICX282AQ, Sony) in the digital camera (DS-5M, Nikon) used for the measurements (after [13]).
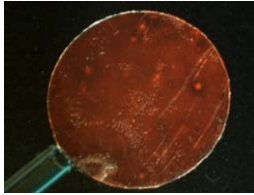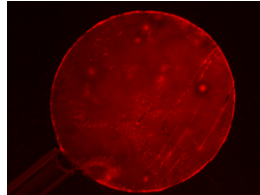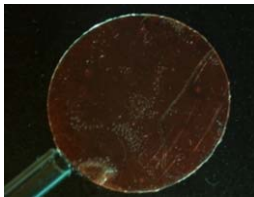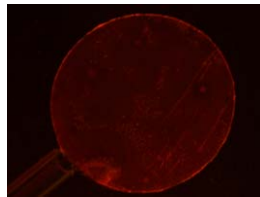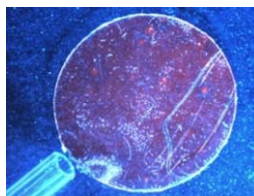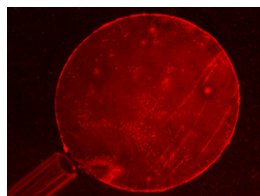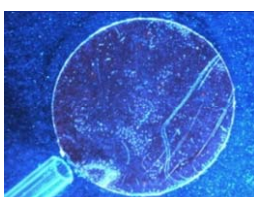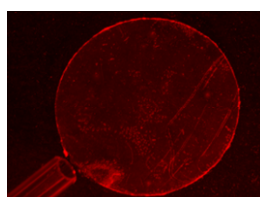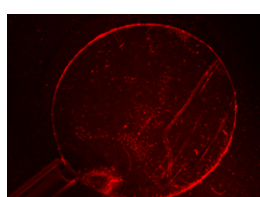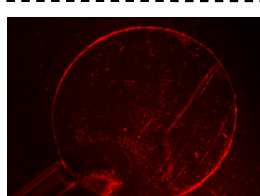
Conditions	O$_2$ (% sat.)	RGB $\Longrightarrow$ R	
Blue excitation with LPF	0		
	100		
Blue excitation without LPF	0		
	100		
White excitation without LPF	0		
	100		

Figure 4. The RGB (red-green-blue total intensity) images of the RedEye[TM] oxygen-sensitive patch (8 mm diameter) and their corresponding R (red intensity) images under blue and white excitation sources with and without long-wave pass filter (LPF) with cut-on wavelength 500 nm.

3.2 Blue Excitation with Long-Wave Pass Filter

The RedEye[TM] was excited by using a blue LED source and the emission from the sensor was detected by a color CCD camera through a long-wave pass filter for this experiment. As described earlier, the original RGB color images were analyzed by the ImageJ program and total color and red color intensities were related with oxygen concentration. The relative emission intensities (i.e., I(0)/I) of the two were plotted in Figure 5 according to Equation (1) of the Stern-Volmer relation. The relative intensities of the RedEye[TM] at 0, 10, 20, 40, 60, 80, and 100% oxygen gas were plotted with error bars which indicate the standard deviation of mean of three independent measurements. The error ranges are so narrow that they are obscured by the symbols. The red color analysis results show a better sensitivity than those of total color analysis for reasons described earlier.

Figure 5. Stern-Volmer plots based on total color (RGB) intensity and red color (R) intensity with blue LED excitation source and long-wave pass filter (error bars: SD of three measurements).

3.3 Blue Excitation without Long-Wave Pass Filter

To evaluate the effect of long-wave pass filter on the measurements, the sensor images were taken without the long-wave pass filter. Figure 6 shows the results. The strong blue hue significantly dominates in the original images taken without the filter as in Figure 4. The total color oxygen sensitivity was degraded accordingly from 2.0 in the previous experiment to 1.2 without filter at 100% oxygen. The red color analysis method, however, effectively compensated this decrease. The relative emission intensity at 100% oxygen gas was 2.0 in red color analysis without optical filter and it is close to that of the total color analysis with optical filter (2.0). Therefore, it can be noticed that the red color extraction from the original images in the absence of an optical filter is as effective as the use of physical optical filter for oxygen measurements.
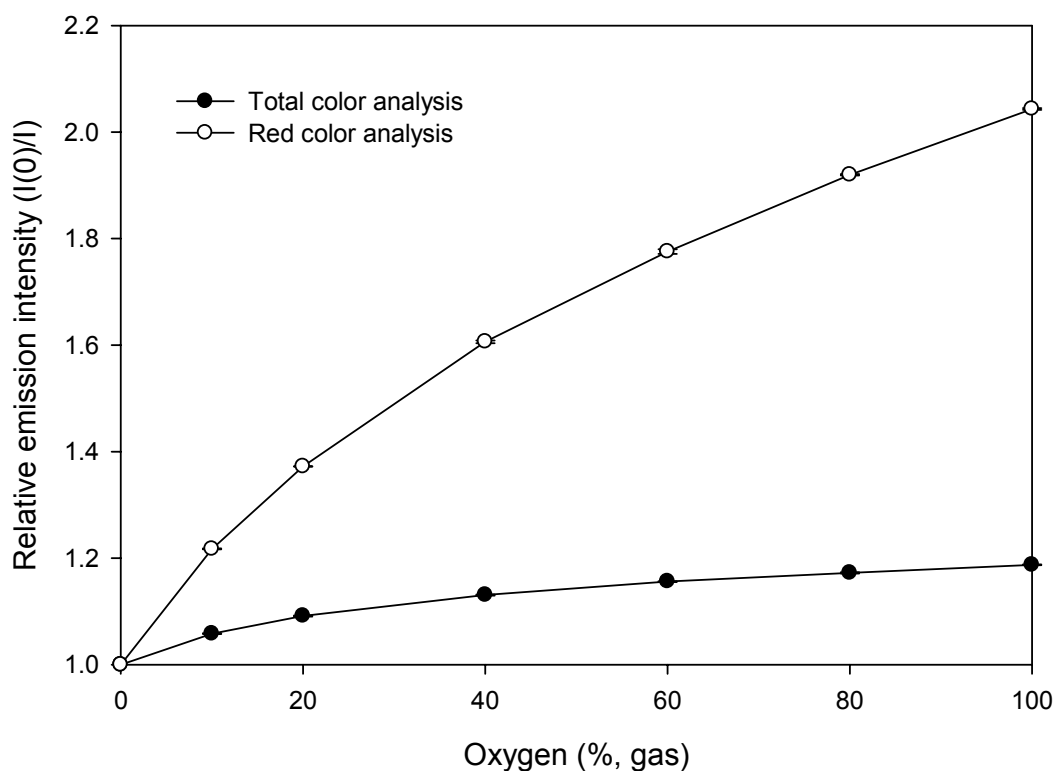
Figure 6. Stern-Volmer plots based on total color (RGB) intensity and red color (R) intensity with blue LED excitation source and without long-wave pass filter (error bars: SD of three measurements).

3.4 White Excitation without Long-Wave Pass Filter

For truly simultaneous structural observation and chemical imaging, the use of same optical instrumentation elements for both purposes is essential. White broad-band light is common for structural observation. It is also useful in the case of multi-analyte chemical imaging because it can be used for multi-luminophore optical sensors which have different excitation wavelength requirement. To check the oxygen measurement efficiency of the sensor patch with white light excitation, the blue LED bulb in the previous sections was replaced by a white LED. The spectral output of the white LED source is plotted in Figure 7 [14] ranging widely from 420 nm to 700 nm. It has a peak output wavelength around 475 nm that is the excitation wavelength required for the oxygen-sensitive patch. This peak output power at 475 nm, however, is very low compared to the blue LED. For this reason, sensitivity degradation to a certain extent is expected when the excitation source is replaced with a white LED as shown in Figure 8. Regardless of the kind of excitation source and the use of long-wave pass filter, the red color analysis method showed better oxygen detection sensitivity. Figure 9 compares the normalized red color sensitivities of the previous three measurement configurations (i.e., Figure 5, 6, and 8). Although the white excitation without filtering shows the least linearity than others, it still exhibits a reasonably good sensitivity without any degradation in the standard deviation. Around 10% of intensity variation was observed when the oxygen concentration was changed from 0% (i.e., anoxic condition) to 20% (i.e., ambient condition) which is the most common and practical range for various biological process monitoring.
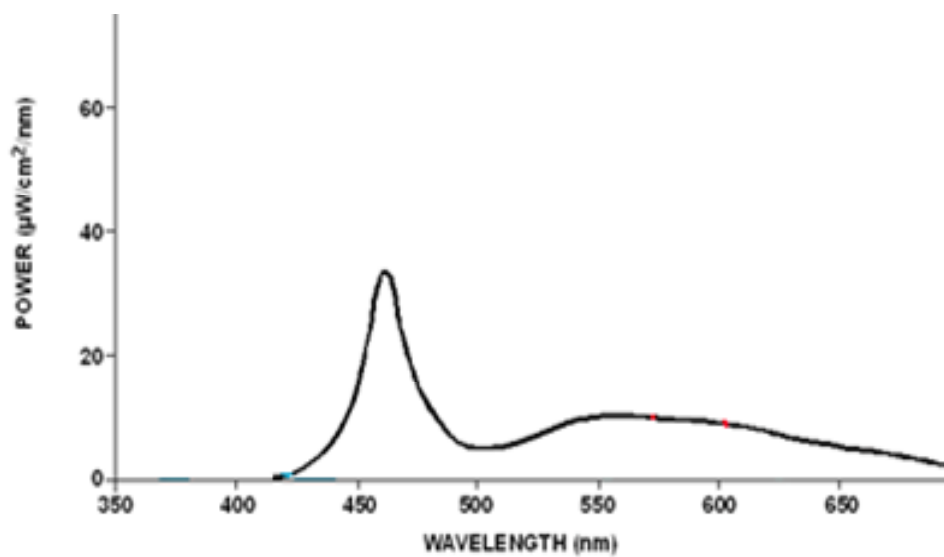
Figure 7. Absolute spectral output of white LED bulb (LED-WHITE, 450~630 nm wavelength, Ocean Optics) (after [14]).
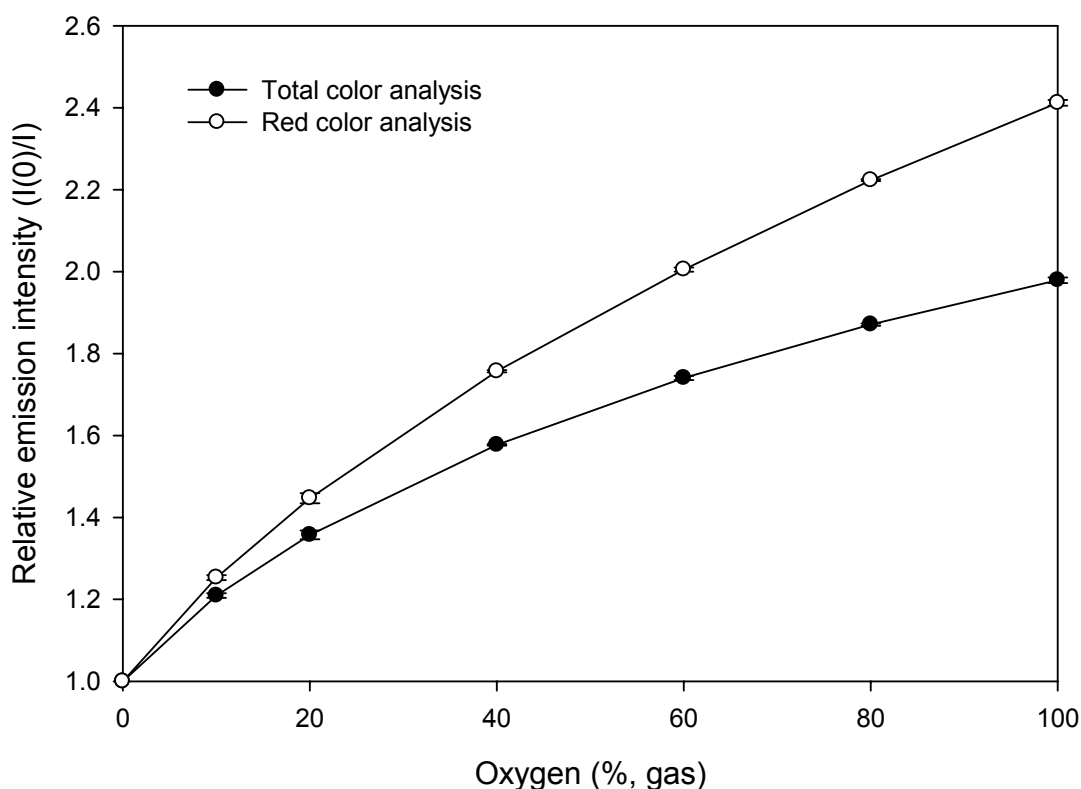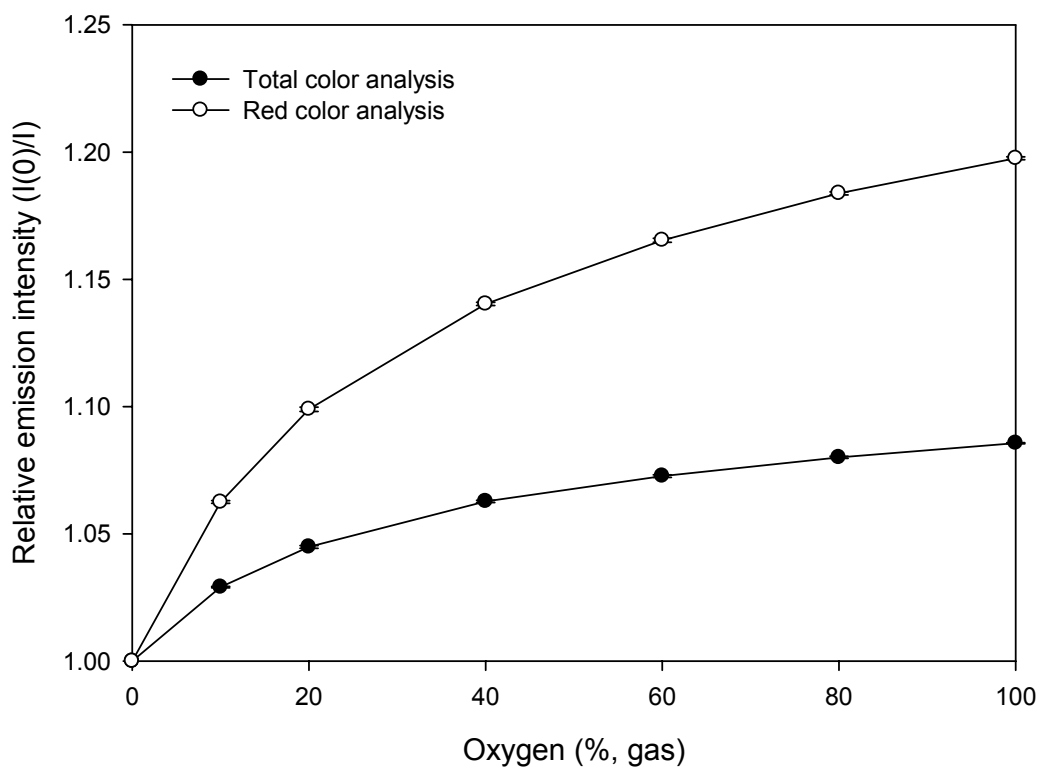

Figure 8. Stern-Volmer plots based on total color (RGB) intensity and red color (R) intensity with white LED excitation source and without long-wave pass filter (error bars: SD of three measurements).
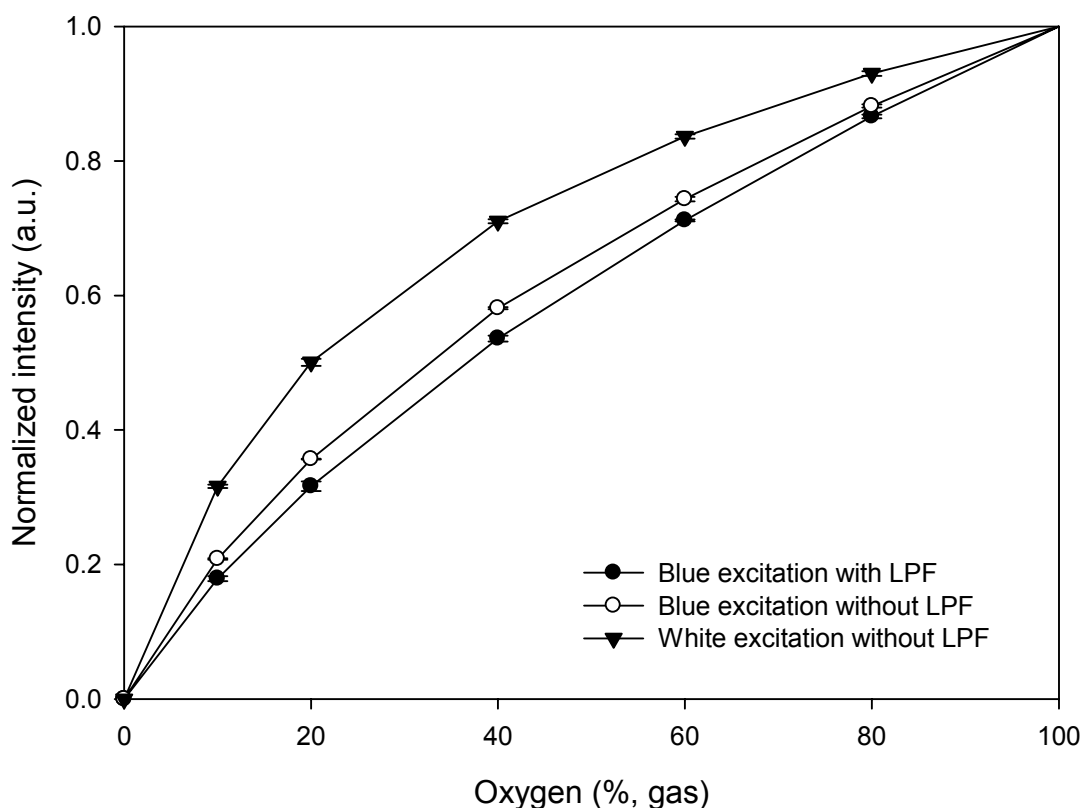
Figure 9. Normalized red color intensity plots to compare the performance of the previous three imaging setups for sensor excitation and optical filtering.

3.5 Comparison of Blue and White Excitation in the Oxygen Gradient Imaging

An oxygen gradient imaging was demonstrated using the RedEye[TM] and oxygen gas flow. Oxygen flow was delivered onto the sensor through a stainless steel tube (0.5 mm diameter) with an incident angle of 2°. Only a part of the oxygen sensor was directly contacted with the oxygen flow to generate an oxygen gradient. The red intensity profile of an image taken without oxygen flow (i.e., 21% ambient air) was subtracted by that of with oxygen flow to cancel out the background which is not related with the oxygen changes as in Figure 10 (a). Figure 10 (b) shows the two-dimensional intensity distribution of the selected region of interest (ROI) in the subtracted image.

Figure 10 (c) shows the normalized line (shown as a dashed line in Figure 10 (b)) intensity profiles of two measurement configurations (i.e., blue excitation with filter and white excitation without filter) and the intensities of ten consecutive pixels were averaged.

(a) Sensor image #1: no flow — Sensor image #2: O$_2$ flow = Sensor image #3: subtracted

(b)

(c)

- ● Blue excitation with LPF
- —— Linear regression of blue excitation with LPF
- ○ White excitation without LPF
- — — Linear regression of white excitation without LPF
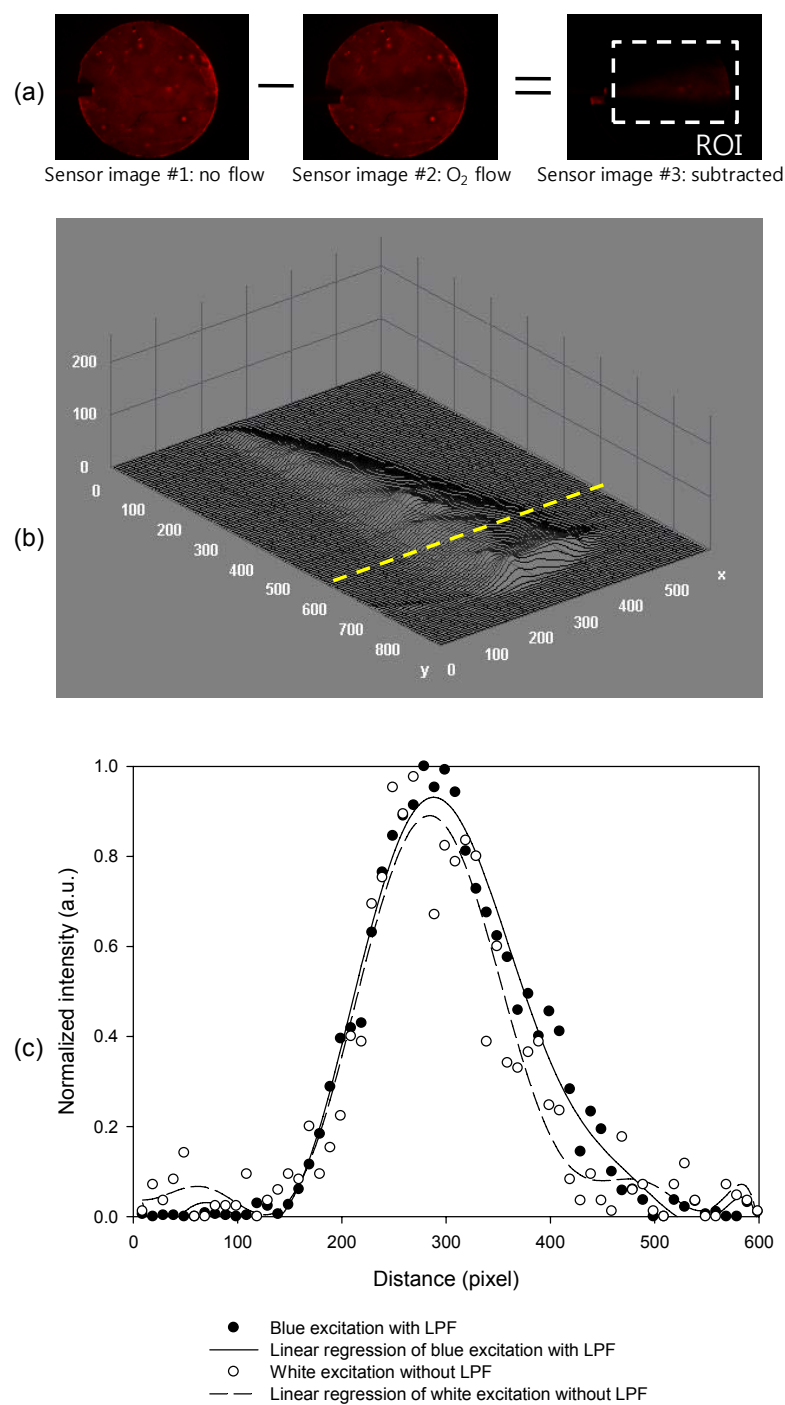
Figure 10. The oxygen gradient imaging. (a) image (with blue excitation and filter) subtraction for the differential intensity profile, (b) plot of the differential intensity from the subtracted image in (a), and (c) normalized intensity profiles along the x-direction (dashed line in (b)). The intensities of ten consecutive pixels were averaged and the 10th order linear regression lines are shown.

Overall, there was good agreement between these two measurements which implies that the white excitation with red color analysis method is effectively mining the oxygen selective information.

4. Conclusion

The red color analysis method was introduced and applied for the gaseous oxygen imaging under the white light excitation. The obtained image was processed by conventional image processing software to extract the red color component from the original RGB color image and to relate it to the oxygen content in the sample. It effectively eliminated the necessity of physical optical filter to improve the sensor sensitivity. Even without using the blue light source and filter, a good sensitivity to oxygen concentration was obtained with the simple red color analysis method. The proposed technique is expected to serve as a simple instrumentation setup and measurement scheme for the simultaneous structural and chemical imaging and multi-analyte detections with a single broad-band light source without filters.

References

[1]   M. Kuhl and L. Polerecky, "Functional and structural imaging of phototrophic microbial communities and symbioses," Aquatic Microbial Ecology, 53, 99-118, 2008.

[2]   R. N. Glud, N. B. Ramsing, J. K. Gundersen and I. Klimant, "Planar optodes: a new tool for fine scale measurements of two-dimensional O2 distribution in benthic communities," Marine Ecology Progress Series, 140, 217-226, 1996.

[3]   G. Holst and B. Grunwald, "Luminescence lifetime imaging with transparent oxygen optodes," Sensors and Actuators B, 74, 78-90, 2001.

[4]   L. Pischedda, J. C. Poggiale, P. Cuny and F. Gilbert, "Imaging oxygen distribution in marine sediments. The importance of bioturbation and sediment heterogeneity," Acta Biotheoretica, 56, 123-135, 2008.

[5]   B. Konig, O. Kohls, G. Holst, R. N. Glud and M. Kuhl, "Fabrication and test of sol-gel based planar oxygen optodes for use in aquatic sediments," Marine Chemistry, 97, 262-276, 2005.

[6]   G. Holst, O. Kohls, I. Klimant, B. Konig, M. Kuhl and T. Richter, "A modular luminescence lifetime imaging system for mapping oxygen distribution in biological samples," Sensors and Actuators B, 51, 163-170, 1998.

[7]   G. Liebsch, I. Klimant, B. Frank, G. Holst and O. S. Wolfbeis, "Luminescence lifetime imaging of oxygen, pH, and carbon dioxide distribution using optical sensors," Applied Spectroscopy, 54, 548-559, 2000.

[8]   J. M. Price, W. Xu, J. N. Demas and B. A. DeGraff, "Polymer-supported pH sensors based on hydrophobically bound luminescent ruthenium(II) complexes," Analytical Chemistry, 70, 265-270, 1998.

[9]   A. Safavi, N. Maleki, A. Rostamzadeh and S. Maesum, "CCD camera full range pH sensor array," Talanta, 71, 498-501, 2007.

[10] J. R. Bacon and J. N. Demas, "Determination of oxygen concentrations by luminescence quenching of a polymer-immobilized transition-metal complex," Analytical Chemistry, 59, 2780-2785, 1987.

[11] M. D. Abramoff, P. J. Magelhaes and S. J. Ram, "Image processing with ImageJ," Biophotonics International, 11, 36-42, 2004.

[12] http://www.datasheetcatalog.org/datasheet/sony/a6803031.pdf. ICX282AQ, August 2009.

[13] K. R. Castleman, "Concepts in imaging and microscopy: color image processing for microscopy," The Biological Bulletin, 194, 100-107, 1998.

[14] http://www.oceanoptics.com/products/ls450.asp. Absolute spectral output for ocean optics LED bulbs, August 2009.

3. An On-Chip Self-Calibration Method of Optofluidic Oxygen Sensor Utilizing Electrolytic Gas Bubbles and a Thin Polymer Membrane

Abstract

A proper *in situ* calibration technology is inevitable to achieve an innovative and autonomous instrumentation for continuous operation without any interruption. However, all *in situ* calibration methods typically require a considerable amount of laborious human intervention and involve bulky mechanical and fluidic components. To solve this problem, electrolytic gas bubbles (i.e., oxygen and hydrogen) method was developed for the *in situ*, on-demand, and on-chip self-calibration of an optical oxygen sensor in this research. Multilayer of dry film resist (DFR) was used for the fabrication of optofluidic sensor assembly. The bubble generating chamber and the sensing chamber were separated by a black hydrophobic membrane for gas diffusion and optical isolation. The optical oxygen sensor and bubble generation electrodes were integrated in the fluidic assembly. The sensor calibration results by external calibrants (i.e., oxygen- and nitrogen-saturated solutions) injection and on-chip bubble generation agreed well. This method is anticipated to enable an on-chip self-calibration of optofluidic oxygen sensor during real-time monitoring.

Keywords

Bubble, optofluidic, oxygen, imaging, self-calibration

1. Introduction

The importance and needs of *in situ* and *in vivo* calibration [1] and self-calibration [2] have been pointed out to achieve innovative and autonomous instrumentations for continuous operation without any interruption. However, little technological breakthrough on a proper *in situ* calibration technology has been made till now. Previous research on sensor self-calibration includes a concept proposed by Demchenko [3]. He

introduced an interesting concept of "OR-OR" switch for the self-calibration of a fluorescence sensor which requires two-band wavelength-ratiometric measurement using rapid reversible single dye molecule. However, sampling from the measurement site for a periodic "gold standard" analysis by reference equipment or injecting external calibrating media are still the most common ways for sensor calibration provided such a single dye molecule is not available in every case. It should be noted that all general concepts of *in vivo* and *in situ* calibration methods require a considerable amount of laborious human attendance and involve externally coupled bulky mechanical and fluidic components.

For the previous work, a self-calibration concept for optical dissolved oxygen sensors [4] and electrochemical glucose/lactate sensors [5] towards reliable and continuous monitoring with minimum human intervention was introduced. These sensors utilized the gas bubbles generated internally. For the two-point calibration of dissolved oxygen sensor, a pair of oxygen and hydrogen bubbles was generated electrochemically within a fluidic channel by a pair of bubble generation electrodes. The electrolysis reactions which take place at the anodic and cathodic bubble generation electrodes are as follows:

$$2H_2O \rightarrow 4H^+ + 4e^- + O_2 \text{ (at anodic electrode)} \tag{1}$$
$$4H_2O + 4e^- \rightarrow 4OH^- + 2H_2 \text{ (at cathodic electrode)} \tag{2}$$
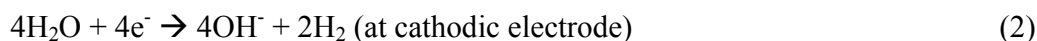
The fiber optic oxygen sensor tip was exposed to local environments depending on the location of the bubbles and the solution. The high-point diagnosis/calibration environment was established within an oxygen bubble (100% oxygen) and the low-point environment within a hydrogen bubble (0% oxygen). In case of enzymatic electrochemical glucose and lactate sensors, the one-point sensor calibration (i.e., zero value) can be performed by manipulating the hydrogen gas bubble. Once the hydrogen bubble is built up, a carefully driven movement of the solution can place the generated bubble over the location of the enzymatic sensor. When the sensor is surrounded by the hydrogen bubble, this oxygen-free environment prevents the oxidase enzyme reaction because of the absence of oxygen. This technique results in mimicking a glucose (or lactate)-free microenvironment regardless of its actual presence in sample solutions. This

previous method, however, may have possible problems such as pH change of the sample solution and unwanted byproducts generation. Also the two-phase fluidic manipulation needs accurate control on fluid pumping which, if not controlled, may lead to bubble clogging in the fluidic channel [6].

To resolve this possible problem, an improved assembly design was introduced for optical dissolved oxygen sensor self-calibration in this research. The bubble generating chamber and the sensing chamber were separated by a black gas permeable polydimethylsiloxane (PDMS) membrane for oxygen diffusion and optical isolation. A PDMS was chosen as diffusion membrane due to its high oxygen permeability [7]. Moreover, the dissolved oxygen sensor (commercial oxygen-sensitive patch) is integrated to the sensor chip instead using externally coupled optical oxygen sensor to implement fully integrated microfluidic system.

Dry film resist (DFR) was originally developed for etching and electroplating processes in traditional printed circuit board (PCB) fabrication. In the recent microfabrication developments, DFR has been widely used as a material for the fabrication of 3-dimensional microfluidic devices because of its advantages such as good adhesion and sealing properties to many different surfaces and flatness over a large area for wafer level bonding. Also the possibilities of quick and highly economical fabrication made DFR to be used as a good alternative to the liquid-phase high aspect ratio photoresists such as SU-8, which has poor adhesion on glass, cracking problems caused by internal stress, and uneven thickness affected by its high viscosity. Volto et al. fabricated DFR based microfluidic networks which act as a cell separation system and a fuel cell reaction chamber [8]. Stephan et al. demonstrated fast prototyping of microfluidic structures using a DFR master for a molding process in the soft lithography [9]. Multilayer of DFR was used for the fabrication of 3-dimensional microfluidic structures in this research. Upper and lower layers were fabricated separately, and sandwiched together with a center structure which consisted of a thin glass layer and a black PDMS membrane for gas diffusion.

2. Materials and Methods

2.1 Oxygen Sensor Assembly

The fabrication steps for the dissolved oxygen sensor assembly are illustrated in Figure 1. After cleaning the slide glass (3'' x 1'', Corning Glass Works) with acetone, methanol, and deionized (DI) water, a thin platinum/titanium film (100 nm/20 nm) was deposited by radio frequency sputtering and patterned by lift-off technique to define the bubble generation electrodes. After the patterning of metal electrodes, sample inlet/outlet holes were drilled on the slide glass using a diamond bit (1/16'').

DFRs (MX5050, 50 μm thick, DuPont) were laminated at room temperature using rubber roller followed by post-lamination bake at 100°C for 45 seconds. Totally 4 layers of DFR were sequentially laminated to make 200 μm thick lower fluidic channel. After the lamination of DFRs, the fabricated structure was aligned with a photomask and exposed to UV light with an energy dose of 140 mJ/cm^2 (5.5 mW/cm^2 at 365 nm for 25 seconds). The UV-exposed structure was then baked (i.e., post-exposure bake) at 100°C for 45 seconds. The pattern was finally developed in a stream (200 ml/min) of 0.75 wt% D4000 developer (RBP Chemical Technology) at room temperature for 20 minutes. Extended development time was required due to the thick structure of DFR. The upper layer fluidic structure was fabricated similar to that of the lower fluidic channel.

For the optical dissolved oxygen sensor, a small segment (1.3 mm diameter) of the commercial oxygen-sensitive patch (RedEye^{TM}, RE-FOX-8, 8 mm diameter, Ocean Optics) was cut using an edge-sharpened stainless still tube (Hypo Tube, HTX-16T-12, Small Parts, Inc.). The RedEye^{TM} contains the oxygen-sensitive ruthenium complex fluorophores immobilized in a sol-gel matrix. The segmented patch was attached onto the upper slide glass surface with a self-adhesive acrylic layer provided on the sensor. As shown in Figure 1, the middle layer of the fluidic assembly includes a black PDMS membrane in a cover glass (CS-24/60, 24 x 60 mm, 150 μm thick, Warner Instrument Corp.). The PDMS (Sylgard 184, Corning) and its curing agent were mixed in the ratio of 10:1 by weight. Then the black PDMS membrane solution was prepared by mixing carbon black powder (Raven 14, 45 nm particle size, Columbian Chemicals) into the prepared PDMS solution in the ratio of 6 : 1 (by weight) as described by O'Donnell et al. [10]. After making a hole which is aligned with the sensing chamber on the cover glass,

the hole was filled with the prepared black PDMS membrane solution with a surgical knife and cured for 15 minutes at 150°C. The thickness of the PDMS membrane is same as that of the cover glass (i.e., 150 μm).

Two DFR layers on each side of the middle cover glass served as an adhesive layer for bonding of both the upper and lower fluidic layers. All the three glass substrates were then bonded together at 100°C. The uncrosslinked DFR on both sides of the middle layer slightly melted at 100°C and served as an adhesive layer for bonding both the upper and lower layers. The increase in the temperature up to 100°C for a short time did not affect the sensor patch. As the final step of fabrication, the entire structure was UV-exposed with an energy dose of 140 mJ/cm^2 (5.5 mW/cm^2 at 365 nm for 25 seconds) followed by post-exposure bake at 100°C for 45 seconds.

	Cross sectional view	Top view
Upper layer	Slide glass / DFRs / RedEye™	Sample inlet/outlet / Sensing chamber / RedEye™
Middle layer	Cover glass / DFR / PDMS black membrane	PDMS black membrane
Lower layer	DFRs / Slide glass / Bubble generation electrodes	Bubble chamber / Electrolyte inlet/outlet / Bubble generation electrode
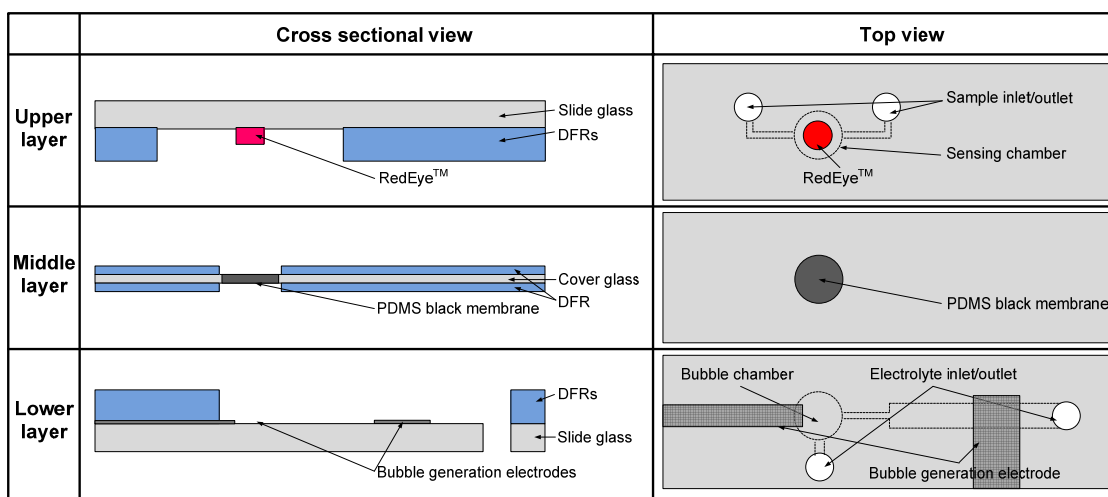
Figure 1. Assembly of the optical dissolved oxygen sensor (RedEye™) module and the self-calibration module. The dry film resist (DFR) layers served as the channel structuring material and the adhesive layers.

2.2 Measurement Setup

Spectroscopic analysis was carried out for the fluorescence detection of the oxygen sensor assembly fabricated. Measurement set up for the fluorescence detection is explained in Figure 2. A spectrometer (USB2000-FLG, Ocean Optics) was used as the detector. A blue LED light source (LS450, peak wavelength 470 nm, Ocean Optics) was used as the excitation source. A reflection probe (R400-7-UV-VIS, Ocean Optics), consisting of six illumination fibers (400 μm diameter each) and one read fiber (400 μm

diameter) was used to capture the luminescence from the samples. All the measurements were performed in a dark environment. The oxygen saturation percentage of the sample solution was regulated by bubbling different ratios of oxygen and nitrogen gases into deionized (DI) water with mass flow controllers (1159B, MKS Instruments) operated by a readout power supply (247C, MKS Instruments). Once the DI water was saturated to a specific level, it was injected into the fabricated sensor assembly with a syringe pump. A current source (225, Keithley Instrument) was used to provide galvanostatic operation to the bubble generation electrodes (i.e., constant current mode). A supporting electrolyte (0.1 M K_2SO_4) was used instead to reduce the voltage between the two electrodes during the bubble generation throughout all the experiments.

Figure 2. The spectrometric optical measurement setup (The distance between the refection probe and sensor spot was optimized to obtain the maximum intensity at emission wavelength (595 nm)).

3. Results and Discussion

3.1 Fabrication

Figure 3 (a) shows the picture of the fabricated sensor assembly and Figure 3 (b) shows the sensor image taken with 0% oxygen saturated sample solution flowing through the fluidic layer. Because of the dark blue color of the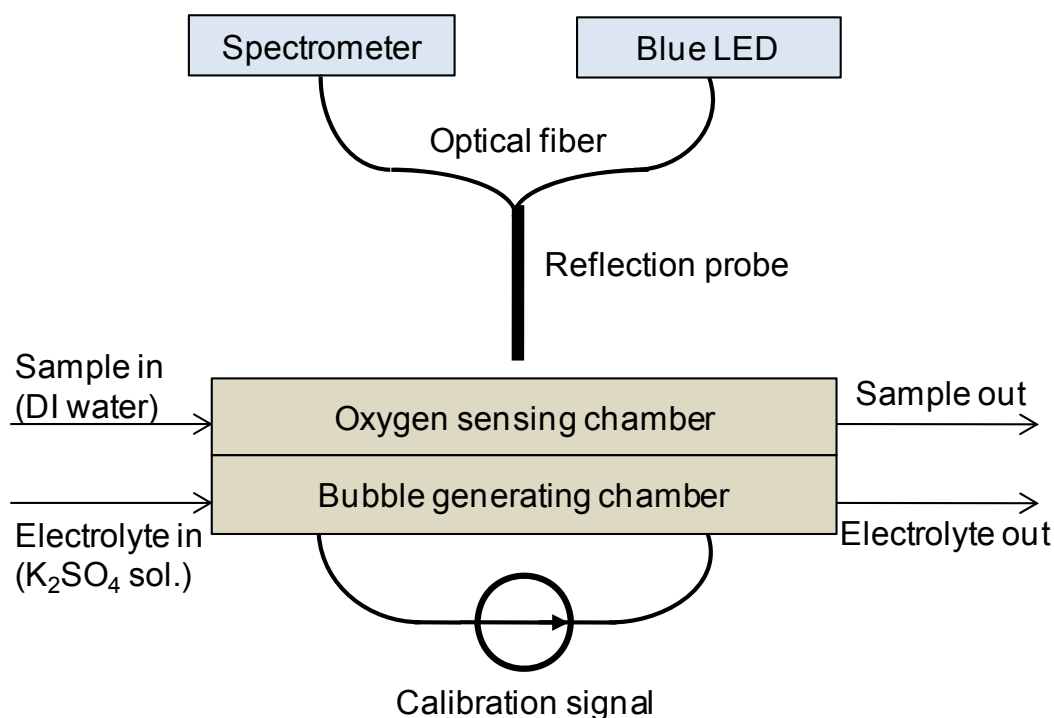 crosslinked DFR, internal fluidic channel could not be seen in the normal ambient light. An intense light was illuminated to see through the channel for better illustration as shown in Figure 3 (a). Cracks in the sensor patch (Figure 3 (b)) were generated after segmenting the sensor patch from its original RedEye^{TM}. Nevertheless, these cracks did not seriously affect the measurements with the reflection probe and spectrometer. No liquid leakage was observed after the injection of the sample solution into the upper sensing chamber and electrolyte solution into the lower bubble generating chamber.

3.2 pH Change Quantification

As the thin PDMS layer serves as a pH change barrier as well as a gas permeable membrane in this assembly, quantification of pH changes in the sample chamber during the bubble generation in the lower chamber is important. During the bubble generation, the environment around the electrode may undergo significant pH changes, either extreme acidic or basic depending on its polarity. No considerable swelling of PDMS membranes has been reported in various acids, bases, and solvents used in organic synthesis [11]. Also a 2-day liquid absorption of PDMS has been investigated by an impedance-based measurement method in various NaOH solutions, and the shift of capacitance versus time was reported [12]. This "capillary effect", however, is not the case when it is to be exposed to acidic or basic environment for short-term (i.e., bubble generation for several minutes). Nevertheless, the fabricated sensor assembly was subjected to actual pH measurement test in order to evaluate the effect of black carbon powder which was added to the PDMS membrane for optical isolation. Figure 4 (a) shows the completed assembly for pH measurement in which the oxygen sensor was replaced by a microcombination pH electrode (AMANI-650, 650 μm tip diameter, 20 mm tip length, Warner Instruments). The pH microprobe was used after the 3-point calibration in 4.0, 7.0, and 10.0 pH buffers. For the chronopotentiometric operation of the

electrode, an electrochemical instrument (FAS1, Gamry Instruments) was used. As seen in Figure 4 (b), no pH changes were observed during each bubble generation (i.e., hydrogen and oxygen) for 10 minutes. The bubble generation current was 10 mA/cm^2 for oxygen generation and -10 mA/cm^2 for oxygen depletion, respectively.
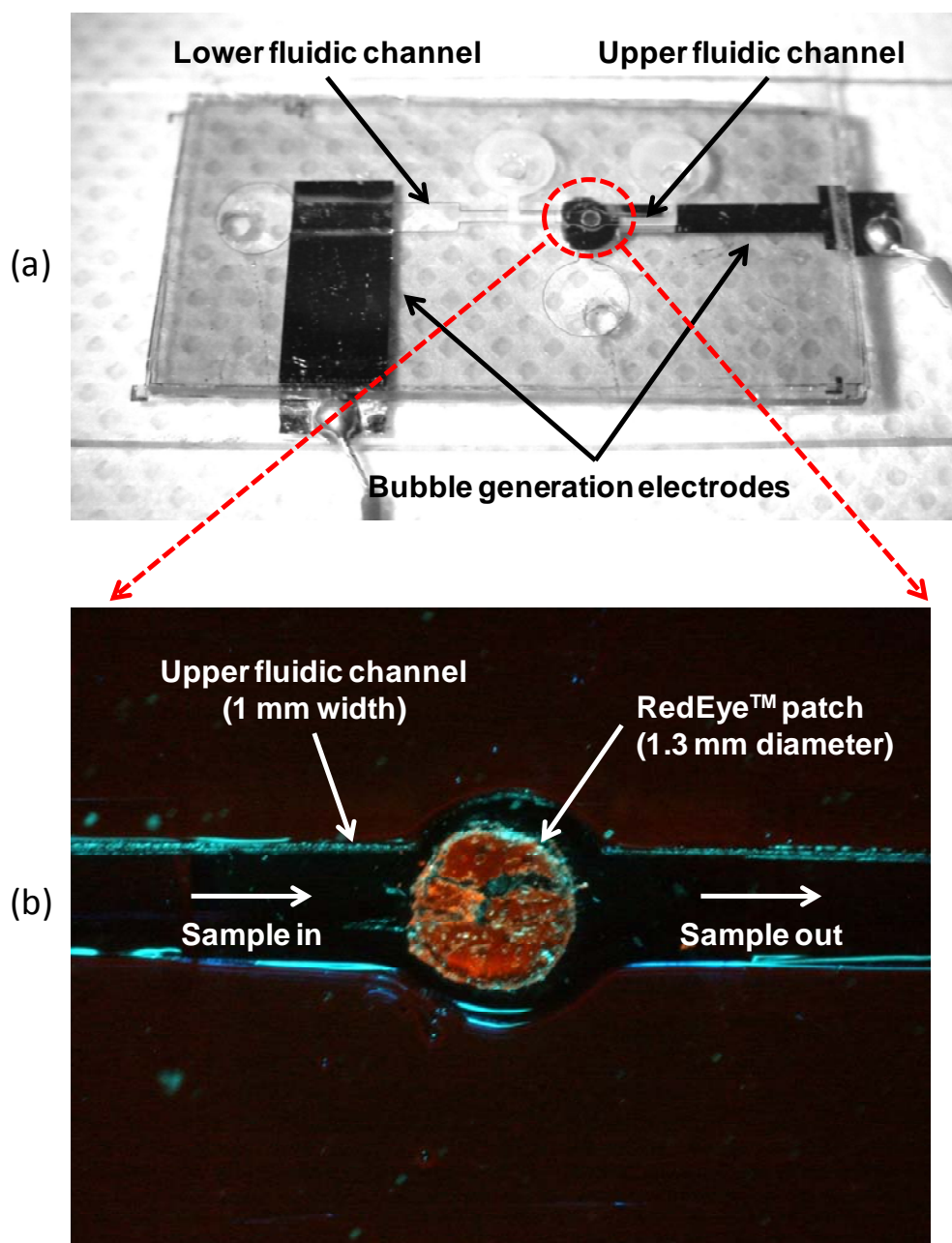

Figure 3. Photographs of fluidic assembly and sensor. (a) fabricated sensor assembly and (b) segmented RedEye^{TM} in the sensing fluidic chamber at 0% oxygen saturated water.

3.3 Dissolved Oxygen Measurements and Bubble Generation for the Sensor
Self-Calibration

The spectra of the RedEye[TM] oxygen-sensitive patch under various oxygen saturations were firstly measured with the reflection probe and spectrometer before the measurements with bubble generation. The emission spectra and typical time response of the RedEye[TM] oxygen-sensitive patch in 0, 10, 20, 40, 60, 80, and 100% oxygen saturated sample solution (DI water) flowing through the fluidic channel are shown in Figure 5 (a) and (b), respectively. The peak emission wavelength of ruthenium complex was at 595 nm, which decreased as the oxygen saturated due to the fluorescence quenching by oxygen. The relative emission intensities (i.e., I(0)/I) of RedEye[TM] spectra peak at 595 nm is plotted in Figure 5 (c) according to Stern-Volmer equation that is the most common way of presenting optical oxygen sensor performance [13].

$$I(0)/I = 1 + K_{SV}[O_2] \qquad (3)$$

where I(0) and I represent the intensities in the absence and presence of oxygen, respectively, K_{SV} is the quenching constant, and $[O_2]$ is the oxygen concentration.

After the spectrometric analysis of oxygen-sensitive patch, the lower fluidic channel was filled with 0.1 M K_2SO_4 electrolyte for bubble generation. The bubble generation current was chosen to be 10 mA/cm^2 for oxygen generation and -10 mA/cm^2 for oxygen depletion, respectively based on previous experience [4]. The spectrometric measurement was interfered by the bubble that was formed under the transparent PDMS membrane possibly due to the scattering of emission. This interference was eliminated by introducing black PDMS membrane that provided an optically isolated condition.

Figure 6 shows a typical time response of the RedEye[TM] oxygen-sensitive patch during the course of iterative on-chip bubble generation and external introduction of calibrating solutions. The sensor readings showed a rapid increase immediately after the start of bubble generation. Between the responses of the two bubbles and two external calibrants, the sensor showed flat responses corresponding to the air-saturated (i.e., 21% oxygen saturation) sample solution. In case of hydrogen bubble generation, for the high intensity point sensor calibration, approximately 5 minutes duration provided a stable

microenvironment with oxygen-depleted condition which is similar to that external nitrogen-saturated sample injection. On the other hand, the response of the sensor reached the steady-state level much faster (about 3 minutes) during oxygen bubble generation, which means the diffusion of oxygen through the membrane to saturate the sensor chamber is easier than consuming the oxygen in the sensor chamber by the electrolysis reactions.
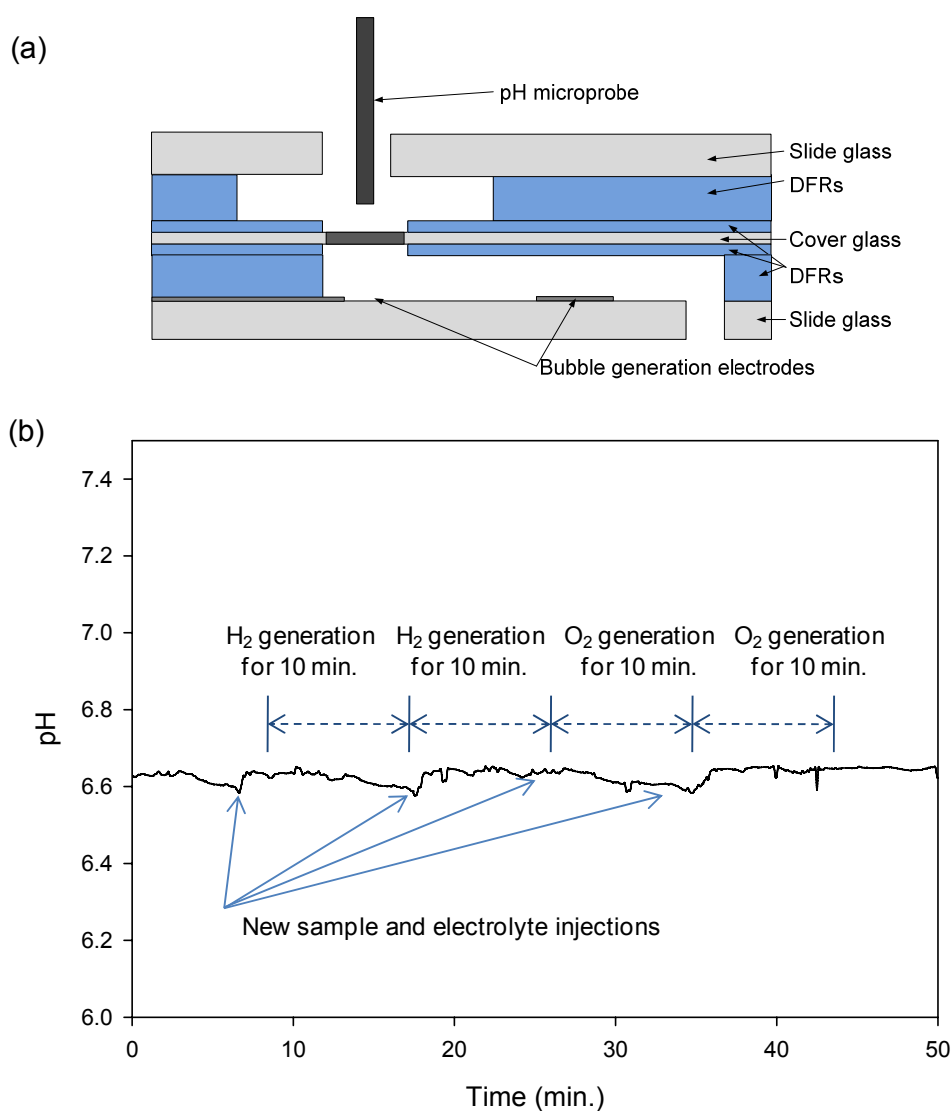
Figure 4. pH measurements during the bubble generation. (a) device cross-section with a pH microprobe (650 μm diameter) mounted and (b) time response of pH during the bubble generation for 10 miniutes. The bubble generation current was 10 mA/cm^2 for oxygen generation and -10 mA/cm^2 for hydrogen generation, respectively.
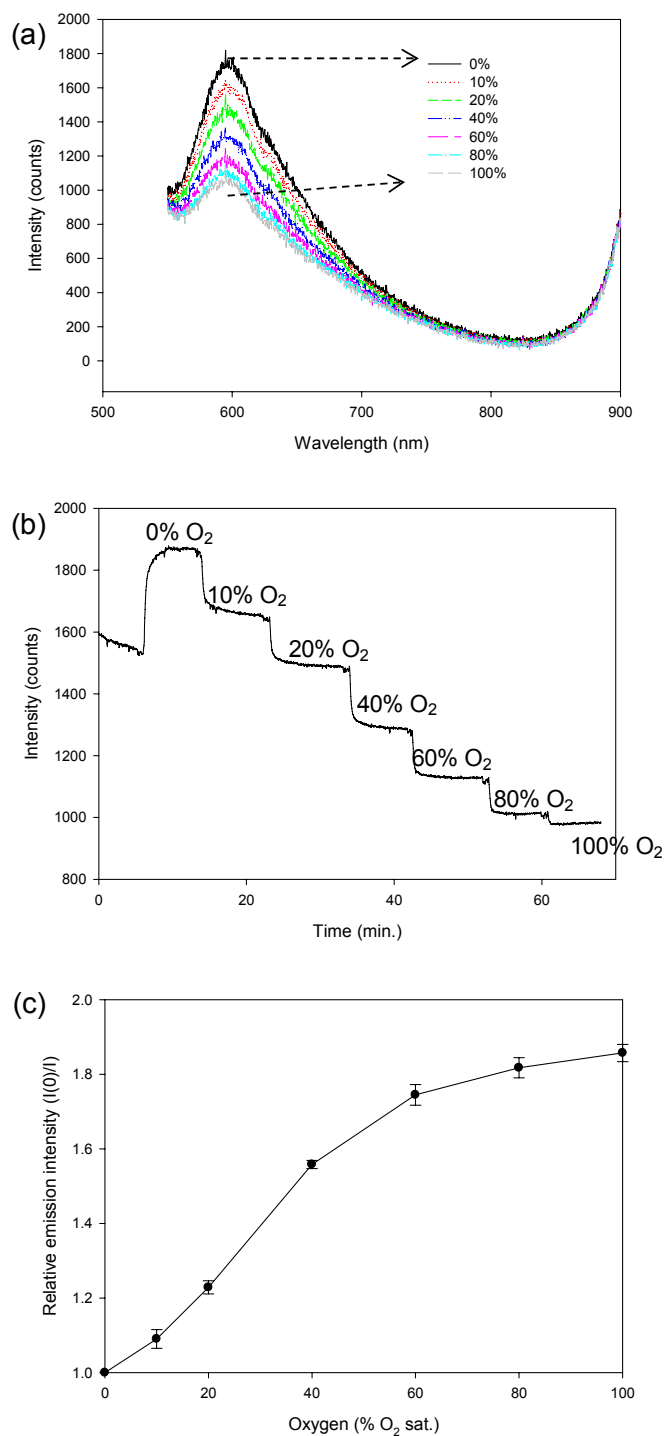
Figure 5. Spectrometric dissolved oxygen measurements using a commercial RedEye[TM] oxygen-sensitive patch. (a) spectra in 0, 10, 20, 40, 60, 80, and 100% oxygen saturated water measured with a spectrometer, (b) typical time response , and (c) Stern-Volmer plot with respect to dissolved oxygen percentage (averages and standard deviations of four measurements).
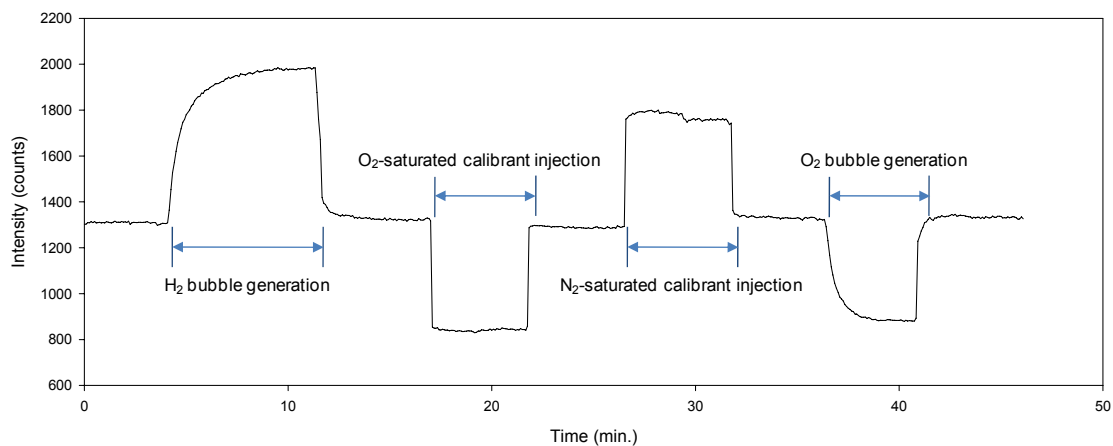
Figure 6. A typical time response obtained during the on-chip bubble generation and the external calibration media injections.

To evaluate the effectiveness of self-calibration of oxygen sensor, Stern-Volmer plots with two methods are compared in Figure 7. For the external calibrants curve, these are the relative emission intensities (i.e., $I(0)/I$) at the peak wavelength (595 nm) when the nitrogen-saturated, air-saturated, and oxygen-saturated samples were externally prepared and injected into the sensor chamber. For the on-chip calibration, they represent the relative emission intensities when the initially air-saturated sample was manipulated by the hydrogen and oxygen bubbles. The sensor calibration using two different methods agrees well in Figure 7, which implies that the diffused oxygen microenvironment established by electrolytic bubbles is effective for on-chip self-calibration. The calibration curve by the on-chip bubbling method is more closely agreed with that of external injection in the range from 0 to 20% which is the most widely used range for various biological process monitoring.
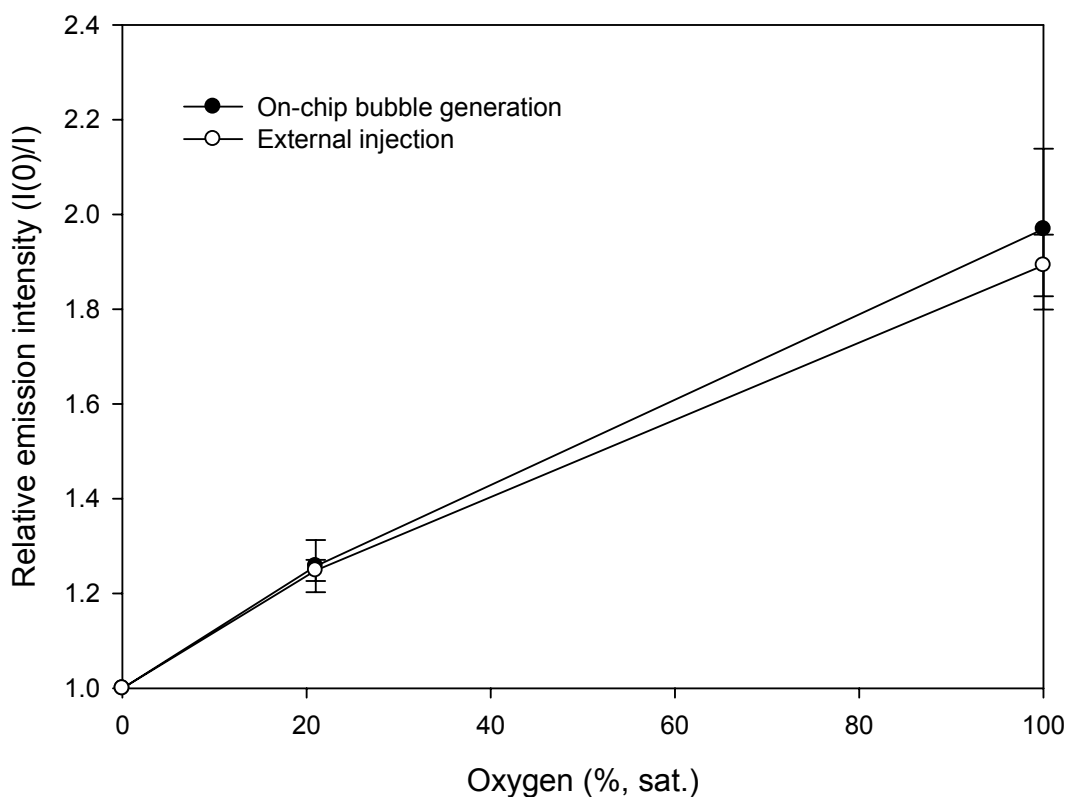
Figure 7. Stern-Volmer plots with respect to dissolved oxygen percentage based on external calibrant injections and on-chip bubble generation for sensor calibration (averages and standard deviations of five measurements).

4. Conclusion

The feasibility of on-demand, *in situ*, and on-chip self-calibration was demonstrated for optical dissolved oxygen sensor. The sensor self-calibration scheme utilized electrochemically generated gas bubbles. The thin black PDMS layer served as a gas permeable membrane and optical isolation component. A pH measurement verified no pH changes in the sensing chamber during the electrolytic bubble generation. The spectrometric results showed good agreement between the two calibration curves with the external calibrating medium injection and with the on-chip gas bubble generation. The proposed technique is expected to be applied to various chemical or biological detections based on the transduction via oxygen including oxidase-coupled biosensors.

References

[1]   P. Rolfe, "In vivo chemical sensors for intensive care monitoring," Medical and Biological Engineering and Computing, 28, B34-B47, 1990

[2]   P. Yager, Biomedical sensors and biosensors, in: B. D. Ratner, A. S. Hoffman, F. J. Schoen, J. E. Lemons (Eds.), Biomatericals Science, Academic Press, pp. 375-388, 1996

[3]   A. P. Demchenko, "The problem of self-calibration of fluorescence signal in microscale sensor systems," Lab on a Chip, 5, 1210-1223, 2005

[4]   J. Park, C. Kim and Y. Kim, "A simple on-chip self-diagnosis/self-calibration method of oxygen microsensor using electrochemically generated bubbles," Sensors and Actuators B, 108, 633-638, 2005

[5]   J. Park, C. Kim and M. Choi, "Oxidase-coupled amperometric glucose and lactate sensors with integrated electrochemical actuation system," IEEE Transactions on Instrumentation and Measurement, 55, 1348-1355, 2006

[6]   M. J. Jensen, G. Goravonic and H. Bruuns, "The clogging pressure of bubbles in hydrophilic microchannel contractions," Journal of Micromechanics and Microengineering,14, 876-883, 2004

[7]   T. C. Merkel, V. I. Bondar, K. Nagai, B. D. Freeman and I. Pinnau, "Gas sorption, diffusion, and permeation in poly(dimethylsiloxane)," Journal of Polymer Science: Part B: Polymer Physics, 38, 415-434, 2000

[8]   P. Vulto, N. Glade, L. Altomare, J. Bablet, L. Del Tin, G. Medoro, I. Chartier, N. Manaresi, M. Tartagni and R. Guerrieria, "Microfluidic channel fabrication in dry film resist for production and prototyping of hybrid chips," Lab on a Chip, 5, 158-162, 2005

[9]   K. Stephan, P. Pittet, L. Renaud, P. Kleimann, P. Morin, N. Ouaini and R. Ferrigno, "Fast prototyping using a dry film photoresist: microfabrication of soft-lithography masters for microfluidic structures," Journal of Micromechanics and Microengineering, 17, N69-N74, 2007

[10]   M. O'Donnell, Y. Hou, J. Kim, S. Ashkenazi, S. Huang and L. J. Guo, "Optoacoustic generation of high frequency sound for 3-D ultrasonic imaging in medicine," European Physical Journal Special Topics, 153, 53-58, 2008

[11]   J. N. Lee, C. Park and G. M. Whitesides, "Solvent compatibility of poly(dimethylsiloxane)-based microfluidic devices," Analytical Chemistry, 75, 6544-6554, 2003

[12]   I. Klammer, M. C. Hofmann, A. Buchenauer, W. Mokwa and U. Schnakenberg, "Long-term stability of PDMS-based microfluidic systems used for biocatalytic reactions," Journal of Micromechanics and Microengineering, 16, 2425-2428, 2006

[13]   J. R. Bacon and J. N. Demas, "Determination of oxygen concentrations by luminescence quenching of a polymer-immobilized transition-metal complex," Analytical Chemistry, 59, 2780-2785, 1987

SECTION

2. CONCLUSION

The dissertation focused on the design, fabrication and characterization of optofluidic biosensor systems for demonstrating the quantitative oxygen imaging with a color CCD camera and the on-chip self-calibration of sensors utilizing electrochemically generated gas bubbles.

Photopatterned PEG hydrogel arrays with embedded Ru-complexes were used as an oxygen detection platform and a color CCD camera was used for luminescence intensity imaging of the hydrogel array. Two methods of color intensity analysis were investigated and compared to quantify the dissolved oxygen content. The first method was to analyze the total RGB color intensity of the original color image. The second method involves extracting the red color element to enhance the sensitivity of oxygen measurement. It was demonstrated that the red intensity analysis method showed improved linearity and sensitivity over the traditional spectrometry and the total color intensity methods by effectively extracting oxygen-related color information. In addition to its performance improvement, the sensor array with the red intensity method offered many other prospective advantages. It allows calibrating individual sensors in an array simultaneously for two-dimensional mapping. The red intensity method can also be adapted to other optical sensors using different luminorphores or to luminescence lifetime and/or phase measurements.

Moreover, the red color analysis method is expected to serve multiple purposes simultaneously such as bare optical imaging and functional imaging when analyzing biochemical samples. The same method was applied to the gaseous oxygen imaging under a simple white light excitation. Even without using the blue light source and filter that has been traditionally used for selective oxygen detection, a good sensitivity to oxygen was obtained with the simple red color analysis method. The proposed technique is thus useful to simplify the instrumentation setup and measurement scheme for the simultaneous structural observation and chemical imaging and multi-analyte detections with a general broad-band light source without filters.

The feasibility of on-demand, *in situ*, and on-chip self-calibration was demonstrated for optical dissolved oxygen sensor for minimal human intervention during continuous operation. The sensor self-calibration scheme utilized electrochemically generated gas bubbles. A thin black PDMS layer served as a gas permeable membrane and optical isolation component. The spectrometric results showed a good agreement between the two different calibration methods with the external calibrating medium injection and with the on-chip gas bubble generation. This method is potentially applicable to the *in situ* calibration procedures of oxygen and hydrogen sensors and to a variety of oxidase-coupled enzyme sensors such as glucose monitors that utilize oxygen as a cofactor of the enzyme reactions. The demonstrated system including the simple and miniaturized calibration module driven by the electrochemical bubble generation principle appears to be one of promising platforms of minimally invasive extracorporeal biosensing devices for long term monitoring.

APPENDIX A

DETAILED PROCEDURES FOR METAL ELECTRODES, FLUIDIC STRUCTURES
AND OXYGEN SENSOR ARRAY

For the bubble generation electrode fabrication, a thin platinum/titanium film (100 nm/20 nm) was deposited by radio frequency sputtering and patterned by lift-off technique as in Table 1.

Table 1. Lift-off procedure for the patterning of bubble generation electrodes.

Process	Used chemicals/Equipments	Procedure
Lift-off resist coating	Lift-off resist (LOR 3A, Microchem) / Spin coater (WS-400B-6NPP/LITE, Laurell Technologies)	- Casting 2.5 ml - Spining at 4000 rpm for 30 seconds (to obtain 3 μm thick)
Positive photoresist coating and soft bake	Positive photoresist (S1813, Shipley) / Spin coater, hot plate (HS40, Torrey Pines Scientific)	- Casting 2.5 ml - Spin at 5000 rpm for 30 seconds (to obtain 1.25 μm thick) - Soft baking at 115°C for 1 minute
Exposure	Mask aligner (CA-800, Cobilt)	- UV dose of 140 mJ/cm^2
Development	Developer (MF-CD-26 , Shipley)	- Immersing for 40-60 seconds for two resists simultaneously
Sputtering	Pt/Ti / Sputter (Discovery-18, Denton)	- Pt/Ti successive deposition (to obtain 100/20 nm)
Lift-off	Remover (Remover PG, Microchem) / Ultrasonic bath (Ultrasonik 14H, Neytech)	- Ultrasonic agitation at 60°C for 20 minutes

Multilayer of dry film resist (DFR) was used for the fabrication of 3-dimensional microfluidic structures and Table 2 shows the related procedure.

Table 2. DFR fabrication procedure for the 3-D microfluidic structures.

Process	Used chemicals / Equipments	Procedure
DFR lamination and post-lamination bake	DFR (MX5050, DuPont) / Rubber roller (4126, Speedball), Hot plate (HS40, Torrey Pines Scientific)	- Laminating DFR at room temperature with rubber roller - Baking at 100°C for 45 seconds - Repeating for 4 layers (to obtain 200 μm thick)
Exposure	Mask aligner (CA-800, Cobilt)	- UV dose of 140 mJ/cm^2
Post-exposure bake	Hot plate	- Baking at 100°C for 45 seconds
Development	Developer (D4000, Shipley), Squeeze bottle	- Developing in a stream (200 ml/min) of 0.75 wt% developer for 20 minutes
Repeating above procedures for both upper and lower fluidic structures		
DFR lamination for center fluidic structures	DFR / Rubber roller	- Laminating DFRs on both upper and lower side of the cover glass at room temperature with rubber roller
Bonding	Hot plate	- Bonding the upper, center, and center structure at 100°C with moderate pressure
Exposure	Mask aligner	- UV dose of 140 mJ/cm^2 for DFR on center structure

The fluorescence quenching of Ru(II)-complexes embedded in photopatterned poly(ethylene glycol) (PEG) hydrogels was utilized as the two-dimensional oxygen detection mechanism for this dissertation. Patterning a thin PEG layer is possible through the addition of a photoinitiator to the PEG-based precursor as in Table 3.

Table 3. Photopatterning procedure for the 2-D PEG hydrogel array.

Process	Used chemicals/Equipments	Procedure
Precursor solution preparation	Dichlorotris(1,10-phenanthroline) ruthenium (II) hydrate 98% (Sigma Aldrich), PEG diacrylate (Mn: 575) (Sigma Aldrich), methanol, toluene, photoinitiator (Darocur 1173, Ciba), deionized (DI) water	- Dissolving Ru(II) complex powder into a mixture of methanol and toluene (4:1, v:v) at a concentration of 5 mg/ml - Mixing the resulting solution (2% v/v) with PEG diacrylate (60% v/v), photoinitiator (2% v/v) and DI water (36% v/v)
Precursor solution injection	Syringe	- Injecting precursor solution into a fluidic chamber
Exposure	Mask aligner (CA-800, Cobilt)	- UV dose of 55 mJ/cm^2
Washing	DI water, squeeze bottle	- Washing unpolymerized precursor solution with running DI water for 1 minute

APPENDIX B

IMAGE PHOTOGRAPHING USING NIKON DS-5M

A color CCD camera (DS-5M, 5-megapixel, Bayer-masked, Nikon) was used for image capturing for this dissertation. CCD cameras are temperature sensitive. The warm up time before photographing was 30 minutes to minimize any thermal instability. The average intensity was consistent over the experimental conditions which makes the CCD camera a good analytical tool for this application. The following tables are the detailed photographing conditions (Table 1) and procedure (Table 2) for the oxygen-sensitive fluorescence imaging with the CCD camera.

Table 1. Photographing conditions for the oxygen-sensitive fluorescence imaging.

Menu	Submenu	Settings
File type	Type	JPEG
	Source (CCD mode)	s5M
	Size (F. Frame)	1280*960
	JPEG quality	Normal
CAM menu	N/A	Advn. (Advanced)
	Display mode	1.3Mi
	Exposure mode	MANU (Manual)
	Shutter speed	Appropriate time depending on the intensity of luminescence (usually 4~12 seconds)
	Contrast	TONE5 (Linear)
	Scene mode	DF/FL (Dark field/fluorescence)
	Photometry mode	Average photometry

Table 2. Photographing procedure for the oxygen-sensitive fluorescence imaging.

No.	Procedures
1	Press focus button.
2	Check the exposure mode has been automatically changed to "MANU".
3	Adjust the shutter speed.
4	Press exposure start button.
5	After the exposure, check a frozen image is displayed in the screen.
6	If necessary, adjust the shutter speed manually, and press exposure start button again.
7	Press capture button to save the image.

APPENDIX C

IMAGE PROCESSING WITH IMAGEJ FOR THE ONE-DIMENSIONAL OXYGEN
SENSOR

The intensities of total color and red color of oxygen sensor images were analyzed by ImageJ. It is freely available, Java-based image processing software developed at the National Institutes of Health (http://rsbweb.nih.gov/ij/). Table 1 shows some of the functions of ImageJ used for the image processing in this dissertation.

Table 1. Image processing procedure with ImageJ.

Menu	Description
File-Open	Load the image.
Edit-Selection-Specify	Set the region of interest (ROI).
Analyze-Histogram	Obtain the total color intensity (usually mean value).
Image-Color-RGB Split	Extract red color intensity.
Process-Image Calculator-Subtract	Subtract one image from another.
Analyze-Plot Profile	Obtain 2-D intensity plot.
Plugins-3D-Interactive 3D Surface Plot	Obtain 3-D intensity plot.
Plugins-Color Inspector 3D	Obtain pixel distribution in 3-D vector space.

APPENDIX D

M-FILE FOR THE IMAGE PROCESSING OF TWO-DIMENSIONAL OXYGEN
SENSOR ARRAY

Although the intensities of total color and red color of oxygen sensor images were analyzed by a freeware ImageJ, an additional custom MATLAB® code was written for convenient analysis of two-dimensional oxygen sensor arrays. Figure 1 shows the image processing sequence for the two-dimensional oxygen sensor array consisted of multiple sensor spots in a single image.
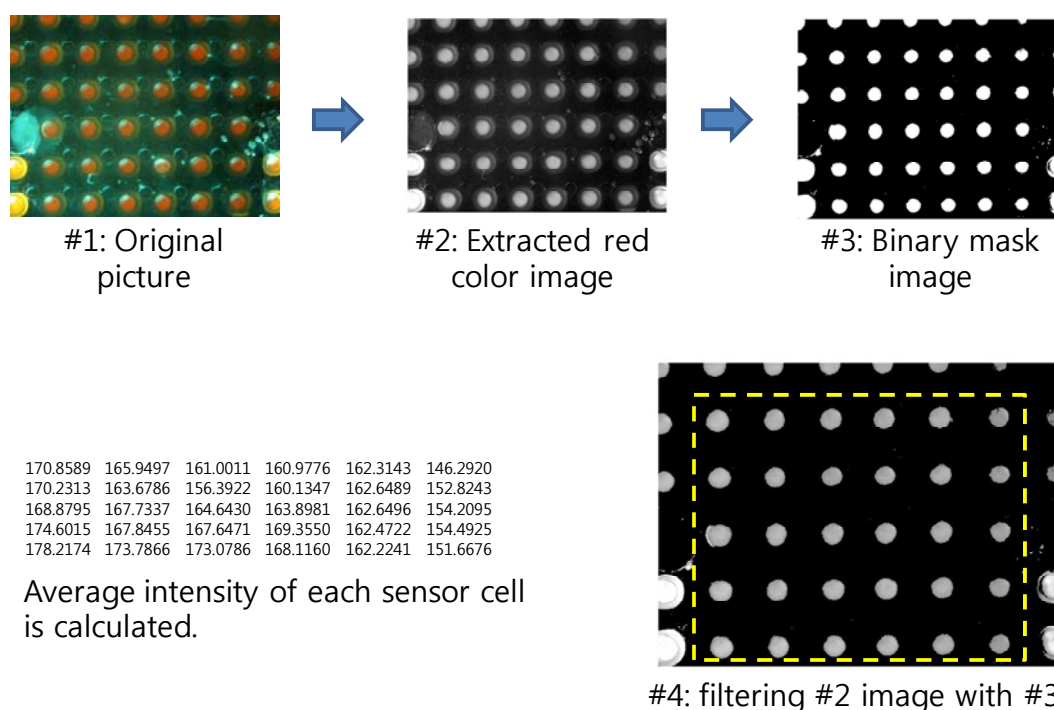

#1: Original picture

#2: Extracted red color image

#3: Binary mask image

```
170.8589   165.9497   161.0011   160.9776   162.3143   146.2920
170.2313   163.6786   156.3922   160.1347   162.6489   152.8243
168.8795   167.7337   164.6430   163.8981   162.6496   154.2095
174.6015   167.8455   167.6471   169.3550   162.4722   154.4925
178.2174   173.7866   173.0786   168.1160   162.2241   151.6676
```

Average intensity of each sensor cell is calculated.

#4: filtering #2 image with #3

Figure 1. Image processing sequence of the two-dimensional oxygen sensor array with MATLAB® m-file.

Once MATLAB® m-file is executed, it asks the numbers of rows and columns of the sensor array which needs to be analyzed. After an input from the user, it will extract the red color component from the original image (#1 and 2 images in Figure 1) and create a binary mask pattern (#3 image in Figure 1) which is thresholded at gray level 25 to create the region of interest (ROI). The threshold level can be optimized by a modification of code depending on the intensity level difference between the sensor spots and the background. If the red extracted image is multiplied by the generated binary mask pattern in the previous step, only the areas of sensor spots area remain as the ROI and background intensity level becomes zero (#4 image in Figure 1). The computer screen

then displays the processed image. The user needs to select each sensor spot area by clicking two diagonal corners of a rectangle that encloses the selected sensor spot. After selecting all sensor spots that need to be analyzed, the average intensities of sensor array will be displayed in the "Command Window" of the MATLAB®.

The MATLAB® m-file for the illustrated image processing is as follows:

```
clear all
close all

% read image
A = imread ('filename.jpg');

% extract red intensity and display processed image
B = A(:,:,1);
imshow(B);

% create a binary mask
BW = (B > 25);
imshow(BW);

% filter the red extracted image with the binary mask to obtain only the sensor spots as a
region of interest
J = immultiply(B,BW);
imshow(J);

% ask how many rows and columns
r = input('How many rows?');
c = input('How many columns?');

L = zeros(r,c);
```

```matlab
% calculate the average pixel intensity of each sensor spot
for i = 1:r*c
    K = imcrop(J);
    S = nonzeros(K);
    T = mean2(S);
    L(i) = T;
end

% show the result as a matrix
disp(L)
```

VITA

Jongwon Park was born on March 5, 1973 in Seoul, South Korea. He received his Bachelor of Science degree from Korea Aerospace University (formerly Hankuk Aviation University) of South Korea, in Aerospace and Mechanical Engineering in 1996. He served as an avionics maintenance officer at the Republic of Korea Air Force (Jul. 1996 – Jun. 1999). After being discharged, he joined Korea Aerospace Industries. Ltd, South Korea, where he worked on the EMI/EMC (Electromagnetic Interference and Compatibility) for T/A-50 aircraft development program (Oct. 1999 – Jun. 2002). He received his Master of Science in Electrical Engineering from Missouri University of Science and Technology (formerly University of Missouri-Rolla) in 2005 and received a Doctor of Philosophy in Electrical Engineering in 2009. He is taking a senior researcher position in the LG Innotek at the Device Laboratory in Ansan, South Korea, starting in Oct. 2009.